

New Developments in Laser-Based Photoemission Spectroscopy and its Scientific Applications: a Key Issues Review

Xingjiang Zhou^{1,4,*}, Shaolong He², Guodong Liu¹, Lin Zhao¹, Li Yu¹ and Wentao Zhang³

¹*Beijing National Laboratory for Condensed Matter Physics,
Institute of Physics, Chinese Academy of Sciences, Beijing 100190, China*

²*Ningbo Institute of Materials Technology and Engineering,
Chinese Academy of Sciences, Ningbo 315201, China*

³*Department of Physics and Astronomy,
Shanghai Jiao Tong University, Shanghai 200240, China.*

⁴*Collaborative Innovation Center of Quantum Matter, Beijing 100871, China.*

**Corresponding author: XJZhou@iphy.ac.cn.*

(Dated: May 30, 2017)

Abstract

The significant progress in angle-resolved photoemission spectroscopy (ARPES) in last three decades has elevated it from a traditional band mapping tool to a precise probe of many-body interactions and dynamics of quasiparticles in complex quantum systems. The recent developments of deep ultraviolet (DUV, including ultraviolet and vacuum ultraviolet) laser-based ARPES have further pushed this technique to a new level. In this paper, we review some latest developments in DUV laser-based photoemission systems, including the super-high energy and momentum resolution ARPES, the spin-resolved ARPES, the time-of-flight ARPES, and the time-resolved ARPES. We also highlight some scientific applications in the study of electronic structure in unconventional superconductors and topological materials using these state-of-the-art DUV laser-based ARPES. Finally we provide our perspectives on the future directions in the development of laser-based photoemission systems.

I. INTRODUCTION

The physical properties of materials are primarily determined by their electronic structures, which are described by the three parameters of the electrons in a solid, namely, energy (E), momentum (k) and spin (s). Angle-resolved photoemission spectroscopy (ARPES), which probes the energy and momentum of electrons simultaneously, is a direct tool in measuring the electronic structure of materials. The spin-resolved ARPES can further detect the spin states of materials. In the past three decades, the ARPES technique has been undergoing dramatic improvements in its performance, making it from a basic band structure mapping technique to a power tool in measuring the many-body effects and electron dynamics in the study of complex quantum materials.

The ARPES technique is based on the photoelectric effect, a quantum phenomenon discovered by Hertz in 1887[1] and theoretically explained by Einstein in 1905 by introducing the quantum nature of light[2]. K. Siegbahn developed photoelectron spectroscopy to study the electronic structure in solids by employing intense X-ray sources and high-resolution electron energy analyzer, which won him the Nobel Prize in physics in 1981[3]. The first demonstration of band mapping by angle-resolved photoemission experiment was realized by Neville Smith et al. in early 1970's[4, 5]. The underlying principle of ARPES is straightforward, as seen in the inset of Fig. 1. The photoelectrons emitted by incident light move in a 2π solid angle surrounding the sample. The electronic structure of the material can be determined from the measured energy and the number of photoelectrons along different emission directions.

According to Einstein's quantum theory of photoelectric effect, electrons in solids are kicked out of materials by the incident photons, and the kinetic energy (E_{kin}) and momentum (p) of the photoelectrons are given by

$$E_{kin} = h\nu - W - E_B \quad (1)$$

$$p = \hbar K = \sqrt{2mE_{kin}} \quad (2)$$

in which $h\nu$ and W are the incident photon energy and the work function of solids, E_B represents the binding energy, K is the wave vector of photoelectrons in the vacuum, and m is the electron mass. The parallel and perpendicular components of p and K are related to the emission angle of the photoelectrons (θ , as defined in the inset of Fig. 1): $p_{\parallel} = \hbar K_{\parallel} =$

$\sqrt{2mE_{kin}} \cdot \sin \theta$ and $p_{\perp} = \hbar K_{\perp} = \sqrt{2mE_{kin}} \cdot \cos \theta$.

The momentum of the electrons in Bloch state inside solids, $\hbar k$, is determined from the measured photoelectrons' momentum p . With a reasonable assumption that the parallel component of the momentum is conserved during photoemission process, the Bloch momentum parallel to the sample surface k_{\parallel} is determined by $|k_{\parallel} + G| = K_{\parallel} = \sqrt{2mE_{kin}} \cdot \sin \theta / \hbar$, in which G is the corresponding reciprocal lattice vector. The momentum of the incident photons is neglected for low-energy photons. The perpendicular component of momentum k_{\perp} cannot be determined directly since the momentum normal to the surface is not conserved because of the broken translation symmetry. In order to determine the value of k_{\perp} , several approaches have been proposed[6]. Since the bulk bands usually show obvious dispersion along k_{\perp} direction, k_{\perp} can be determined from the periodic dispersions along this direction by photon-energy-dependent photoemission measurements. One way is to compare experimental band dispersions with the calculated results at different k_{\perp} and find out the proper value of k . The other way is based on the assumption of a free electron final state. In this case, the value of k_{\perp} can be determined as:

$$k_{\perp} = \sqrt{\frac{2m}{\hbar^2} [(h\nu - W) \cos^2 \theta + V_0]} \quad (3)$$

where m is the electron mass, W is the work function and V_0 is the so-called inner potential. Once the inner potential V_0 is determined from the photon-energy-dependent measurements, the value of k_{\perp} can be determined. By measuring the energy and intensity of photo-emitted electrons at different emission angles, ARPES is able to map the band structure, namely, determining both the energy and momentum of the electrons in solids.

Under sudden approximation, ARPES measures the single particle spectral function that is the imaginary part of the Green's function $G(k, \omega)$ [7-10],

$$A(k, \omega) = -\frac{1}{\pi} \text{Im} G(k, \omega) \quad (4)$$

The Green's function is expressed as

$$G(k, \omega) = \frac{1}{\omega - \varepsilon_k - \Sigma(k, \omega)} \quad (5)$$

Then the single particle spectral function can be written in terms of electron self-energy $\Sigma(k, \omega) = \Sigma'(k, \omega) + i\Sigma''(k, \omega)$ where $\Sigma'(k, \omega)$ and $\Sigma''(k, \omega)$ are the real and imaginary parts, respectively:

$$A(k, \omega) = -\frac{1}{\pi} \frac{\Sigma''(k, \omega)}{[\omega - \varepsilon_k - \Sigma'(k, \omega)]^2 + [\Sigma''(k, \omega)]^2} \quad (6)$$

In the photoemission process, $A(k, \omega)$ can be obtained by measuring the photoelectron intensity as a function of energy and momentum:

$$I(k, \omega) = I_0(k, \nu, A) f(\omega) A(k, \omega) \quad (7)$$

where k is momentum, ω is energy relative to the Fermi level, $I_0(k, \nu, A)$ is proportional to the matrix element $|M_{f,i}^k|^2$ which is related to the momentum of electrons (k), the energy (ν) and polarization of incident photons[6, 11]; $f(\omega) = (e^{\omega/k_B T} + 1)^{-1}$ is the Fermi-Dirac distribution function which indicates only occupied states are probed in the photoemission process. By analyzing the measured $A(k, \omega)$ with the spectral function in Eq. 6, the real and imaginary parts of the electron self-energy can be extracted to study the many-body effects in solids, i.e., how electrons interact with other entities like electrons, phonons and etc. In the early time, because of limited energy and momentum resolutions, the application of ARPES is mainly limited to measure the gross band structure of materials. Since the late 1980s, the performance of ARPES has been dramatically improved thanks to the discovery of high temperature cuprate superconductors, followed by further exploration of the strongly correlated electron systems. ARPES has been developed into a leading experimental tool in condensed matter physics[11–13].

The principle of a modern ARPES is schematically shown in Fig. 1. The sketched hemispherical electron energy analyzer is equipped with a two-dimensional spatially-resolved detector and a multi-element electrostatic input lens. When it is operated in the angle-resolved mode, the photoelectrons within an angular span of ~ 30 degrees along a window defined by the entrance slit (along x direction in Fig. 1) are collected by the angle-resolved lens and then spread to different positions along the x axis of a two-dimensional detector. Meanwhile, the photoelectrons are dispersed along the y axis of the detector as a function of their kinetic energy after passing through the hemispherical deflector. The combination of the angle-resolved lens and the two-dimensional detector makes it possible to measure multiple photoemission spectra simultaneously from different photo-emitting angles, obtaining a two-dimensional snapshot of photoelectron intensity as a function of energy and momentum (Fig. 1)[14, 15]. This multiple-angle collection of photoelectrons is a big jump of the ARPES technique from the previous one-angle-at-a-time measurement. In addition to the dramatic improvement of data acquisition efficiency, the energy and momentum resolutions of the modern electron energy analyzers are also significantly improved; the typical energy

resolution and angular resolution are better than 1 meV and 0.1 degree, respectively.

There are always strong demands in improving the performance of ARPES, including the energy and momentum resolutions, the data acquisition efficiency, and the stability of the system. The increasingly rich and deep physics in condensed matter physics pushes ARPES further to probe fine electronic structure under extreme conditions. For example, it is still a challenge for ARPES to measure the superconducting gap of Sr_2RuO_4 with a superconducting transition temperature $T_c \sim 1$ K[16] and some heavy Fermion superconductors, taking CeCoIn_5 of a T_c at 2.3 K as an example[17]. The latest improvement of the ARPES has promoted it from a conventional band mapping tool to a cutting edge probe of the many-body effects in quantum materials[13]. However, further improvements are urgently needed. Since the photon source plays a key role in dictating the ARPES performance, great efforts have been made to develop better photon sources such as the synchrotron radiation light and monochromatic light from gas-discharge lamps. The newly developed deep ultra-violet (DUV)(including ultra-violet(UV) and vacuum ultra-violet(VUV)) lasers are a novel and powerful source for the ARPES experiments[18–22]. The DUV laser light sources have enabled ARPES with superior and unique advantages, pushing the photoemission technique to a new level and leading to tremendous high-quality and significant works in studying the fine electron structure of complex quantum materials such as unconventional superconductors and topological materials.

Generating a quasi-continuous-wave (CW) VUV laser light with a photon energy of $h\nu = 6.994$ eV by the second harmonic process using $\text{KBe}_2\text{BO}_3\text{F}_2$ (KBBF) nonlinear crystal, VUV laser-based ARPES systems with an energy resolution better than 1 meV were developed[21, 22]. In the last decade, several other VUV laser-based photoemission systems have been developed. In this brief review, we will cover the efforts in developing a series of VUV laser-based ARPES: (1). VUV laser-based ARPES with super-high energy and momentum resolutions. (2). VUV laser-based spin- and angle-resolved photoemission spectroscopy(SARPES). (3). VUV laser-based angle-resolved time-of-flight photoemission spectroscopy(TOF-ARPES). (4). VUV laser-based time-resolved ARPES (tr-ARPES). We will highlight some scientific applications in the unconventional superconductors and topological materials by using these state-of-the-art VUV laser-based ARPES systems. Finally, we will provide some perspectives on future directions of the laser-based ARPES techniques.

II. THE DEVELOPMENT OF VUV LASER LIGHT SOURCE FOR PHOTOEMISSION SPECTROSCOPY

A. Basic Considerations of Laser Light as a Light Source

Laser light source seems to be a natural choice for photoemission technique. Historically, laser light used as a photoemission light source can be traced back to very early time, mostly for time-resolved experiments[23, 24], including two-photon photoemission[25–27]. The laser light was generated by using second-harmonic generation (SHG) in nonlinear optical crystal or high harmonic generation (HHG) technique in noble gas. Due to poor energy resolution, low repetition rate, low photon flux of the laser systems and the old-fashioned electron energy analyzers, these early laser-based photoemission techniques are hard to provide information on the intrinsic electronic properties of the measured materials. Until quite recently, near-ultraviolet (NUV) solid state source and HHG gas source became practical in the time-resolved pump–probe ARPES[28–31]. However, it is still impossible for these laser light sources to achieve super-high energy resolution on the order of a few meV.

There are a number of basic requirements for a laser light to be used for a high resolution ARPES system:

(1). Proper photon energy: First, for the photoemission process to occur, the photon energy must be large enough to overcome the usual 4~5 eV work function of the material under measurement. The laser light must have a photon energy larger than 5 eV. Second, lower photon energy is desirable to achieve an enhanced bulk sensitivity, high photoemission cross section, reduced extrinsic background, high momentum resolution and a better selectivity in perpendicular wavevector k_{\perp} . For the photon energy between 20 and 100 eV frequently used in ARPES measurements, the mean free path of the photoelectrons is typically $< 10\text{\AA}$ [32], which renders the technique rather surface sensitive. For the lower photon energy between 6 and 15 eV, the corresponding electron mean free path is enhanced to $\sim 20\sim 100\text{\AA}$ depending on the material[20, 21, 32]. Third, one should consider the momentum space that can be covered at a given laser photon energy; lower photon energy will lead to a limited momentum space. Taking all the above factors into consideration, a possible proper range of photon energy for a super-high resolution ARPES can be 6~15 eV.

- (2). High photon flux: The laser light must have high enough intensity in order to get decent photoemission signal to achieve sufficiently high signal-to-noise ratio and high data acquisition efficiency;
- (3). Narrow bandwidth: The bandwidth of the laser light will be a major factor in determining the overall instrumental energy resolution. To get high energy resolution, a narrow bandwidth of the laser light is necessary.
- (4). Continuous-wave (CW) or quasi continuous-wave laser light source: Photoemission process involves the space charge effect that may shift the energy position, broaden the linewidth and distort the lineshape of the photoemission spectra[33–35]. This effect becomes prominent when there is a large number of photons in one pulse, such as in the pulsed laser. It is preferable to use CW or quasi-CW laser light (~ 100 MHz) in order to minimize the space charge effect to get high energy resolution and intrinsic signal.
- (5). Compatible electron energy analyzer: The relatively low kinetic energy of photoelectrons when using laser light puts a stringent demand on the electron energy analyzer. First, it requires the angular mode of the electron energy analyzer to work properly at such a low electron kinetic energy. Second, it should have a super-high energy resolution in order to take full advantage of the narrow bandwidth of the laser light[21, 22].
- (6). Variable polarizations: Controllable polarizations of laser light can be used to take advantage of the photoemission matrix element effect and disentangle the orbital characters of the energy bands[6, 11]. The circular polarizations can be used to study magnetism or test time-reversal symmetry breaking.
- (7). Variable (< 1 mm) beam spot size: Small spot size is desirable for improving the performance of the electron energy analyzer and measuring on a small area of samples. On the other hand, small spot size tends to give rise to strong space charge effect. In order to get a good balance and depending on different materials measured, it is helpful to be able to tune the laser light spot size.
- (8). Long term stability: Laser light source should be stable during the ARPES measurements that usually last for a couple of days.
- (9). Compact and simple construction: This will lead to a considerable reduction in building and operating costs as well as lab space requirements.

For the time-resolved ARPES (tr-ARPES), in addition to the requirements listed above,

the pulse duration, the repetition rate, and the wavelength tunability of the laser light should also be considered[36].

B. Generation of Laser Light for Photoemission

In general, the UV and VUV laser light required for the photoemission process can be generated through various frequency up-conversion techniques that are primarily divided into two categories. One utilizes the second order nonlinear processes (second harmonic generation, SHG) in the non-linear optical crystals (NLOC) to produce deep-UV laser light. These laser light sources are mainly used in the high-resolution ARPES system[20–22, 37–41]. The other is based on the higher order nonlinear processes (high harmonic generation, HHG) in the noble gases to generate extreme ultra-violet (EUV) and even X-ray ultra-violet (XUV) laser light. Such a short wavelength radiation is mostly used in the tr-ARPES apparatus[24, 30, 42–45]. Usually the second-order nonlinear process has a higher generation efficiency than the HHG in noble gas. Recently, free electron laser (FEL) has emerged as a versatile light sources for the tr-ARPES as the probe beam. Table I lists some typical types of laser light source used for ARPES systems.

Both SHG in crystals and HHG in noble gases originate physically from the nonlinear optical process (NLO) in which high intensity laser light interacts with a nonlinear media, that is, the dielectric polarization P responds nonlinearly to the electric field E of the light.

$$P(t) = \varepsilon_0(\chi^{(1)}E(t) + \chi^{(2)}E^2(t) + \chi^{(3)}E^3(t) + \dots) \quad (8)$$

where the coefficients $\chi^{(n)}$ are the n^{th} order susceptibilities of the medium. In general, $\chi^{(n)}$ is an $(n + 1)^{th}$ -rank tensor. As a noble gas atom is centrally symmetric, the even order susceptibilities become zero. For HHG in gas, only odd multiple of the fundamental frequency can be produced. While for the non-central symmetric crystals, $\chi^{(2)}$ does not equal to zero, so SHG can take place. Fig. 2a-e schematically shows the working principles of different laser sources that are utilized in ARPES laboratories all over the world[20–22, 24, 30, 38–51].

1. SHG: Solid State Deep UV Laser light source

The most popular and reliable approach is to employ the SHG technique to realize a deep-UV laser light source for ARPES application. This technique is easy to implement because the laser light beams do not need to be separated and overlapped spatially and temporally [20–22, 38–41, 46–49]. The most important (key) element is the NLO in the frequency up-conversion of the solid state laser light source. Specifically, SHG can be described by the following equation.

$$P = \alpha E + \beta E^2 = \frac{1}{2}\beta E_0^2 + \alpha E_0 \cos(\omega t) + \frac{1}{2}\beta E_0^2 \cos(2\omega t) \quad (9)$$

Under the non-depleted pump approximation[52], the theoretical VUV output power can be calculated by the following formula.

$$P_{2\omega} = \frac{8\pi^2 d_{eff}^2 L^2 I_\omega}{\varepsilon_0 n_\omega^2 n_{2\omega} c \lambda_\omega^2} P_\omega \quad (10)$$

where d_{eff} is the effective NLO coefficient of an NLO crystal; L is the optical path in the crystal; I_ω is the peak power density of the fundamental beam in NLO crystal; ε_0 is the vacuum permittivity, n_ω and $n_{2\omega}$ are the refractive indices of NLO crystal at frequency ω and 2ω ; c is the light speed in vacuum, λ_ω is the fundamental wavelength, and P_ω and $P_{2\omega}$ are the powers of ω and 2ω beams, respectively.

A VUV NLO crystal that generates laser light applicable for photoemission should have a high NLO coefficient, a short absorption edge below 200 nm, and a moderate birefringence (0.07~0.10). Fig. 3 summarizes the shortest second-harmonic generation SHG wavelength available for the typical and well-developed NLO crystals[21]. Although BaB₂O₄ (BBO) and LiB₃O₅ (LBO) are usually used for SHG from visible to ultraviolet all the way to 200 nm, their performance below 200 nm is rather poor. In the case of BBO, since the absorption edge is at 189 nm, it can only achieve SHG output not shorter than 210 nm. For LBO, although the transparent range is wide, the phase matching is limited by its small birefringence. As a result, the shortest SHG output wavelength of LBO is only 276 nm under phase-matching conditions.

Figure 2a schematically shows a ~6 eV laser light generation that has become a popular and robust solution of light source in many lab-based tr-ARPES and high resolution ARPES systems[20, 37–41]. This approach commonly utilizes a cascade of two frequency doubling

stages in nonlinear BBO crystals through type I phase matching. The first SHG laser light is used as the input of the second harmonic stage. Finally, the ~ 200 nm UV laser light can be achieved through the fourth harmonic generation ($2\omega+2\omega$: FHG) out of a ~ 800 nm Ti:sapphire laser light with a high repetition rate of hundreds of kHz or MHz. Basically, a lower-limit wavelength 205 nm is restricted by the phase matching condition in this scheme.

KBBF is a novel UV NLO crystal that can break the 200 nm wavelength barrier and enter the VUV region. It has a large NLO coefficient of $d_{11} = 0.49$ pm/V, good birefringence of $n=0.072$, and a very short transmission cutoff wavelength of 152 nm. So far, it is the only crystal available that enables phase matching below 160 nm for SHG. However, a major obstacle of using KBBF lies in its platelike nature. It is difficult to grow large-sized KBBF crystal that is suited to be cut at the phase-matching angle. To solve this problem, Chen et al. developed a prism-coupled technique (PCT) device, as schematically shown in Fig. 4[53], which is composed of a KBBF crystal sandwiched in between two CaF_2 prisms, or one SiO_2 and one CaF_2 prism, with a proper apex angle. By using this KBBF-PCT device, laser light with 172.5 and 163.3 nm wavelengths have been demonstrated which are the shortest achieved so far by nonlinear crystals for SHG and sum-frequency mixing (SFM), respectively.

Recently, the continuous-wave laser light sources have also been developed and used in ARPES experiments as reported for a 6.05 eV (205 nm) laser light source[37]. The CW laser light used in ARPES has two additional advantages: one is the extremely narrow bandwidth of the light due to its infinite pulse duration; the other is theoretically zero space charge effect. CW laser light sources based on KBBF with a power level of 1.3 mW at 191 nm (6.49 eV)[54] and 15 mW at 193 nm (6.43 eV)[55] have also been reported. The ~ 190 nm laser light source can cover larger momentum space than that by 205 nm (6.05 eV) laser light in ARPES measurements.

2. High Harmonic Generation

VUV or EUV laser light sources based on HHG process have been widely used in the tr-ARPES experiments, producing a lot of significant results in unveiling the non-equilibrium dynamics of electrons in charge-density-wave (CDW) materials, magnetic surface, and ultra-fast atom-specific electronic dynamics[30, 43, 56]. The HHG process occurs in a gas cell or

gas jet when the noble gas atoms are illuminated by a near-IR laser beam or near-UV laser beam and sometimes their combination with the intensity reaching up to 10^{14} W·cm $^{-2}$ in the infrared regime. The earliest observation of this phenomenon is back to 1990s[57]. The basic mechanism can be qualitatively described by a 3-step process[43, 58]. In the first step, the bound electron becomes free after being ionized by the high electric field of the laser light through multi-photon ionization or tunnel ionization processes. Second, the electron is accelerated by the laser light field and then returns to the vicinity of its parent ion when the laser light field reverses. Third, the electron may recombine with the ion, emitting an high energy photon. Its energy is an odd multiple of the IR photon energy. The recombination usually has a very low probability on the order of 10^{-6} . It leads to an extremely low frequency up-conversion efficiency from IR to XUV laser light.

In the HHG process, the maximum achievable photon energy is limited only by the kinetic energy that the electron can accumulate during the optical half cycle[58]. Therefore, such a process is most effective with few-cycle femtosecond pulses operating at a lower repetition rate of about 1-100 kHz. Since HHG is a highly nonlinear process, the efficiency and the cut-off energy depend sensitively on a number of experimental factors[43, 58], including gas species and pressure, laser light properties (wavelength, the pulse width, power and repetition rate), and the focusing conditions (beam profile, the focusing geometry and the interaction length).

It is worth mentioning that a laser light source with a photon energy of 11 eV was recently developed which combines the merits of narrow bandwidth in solid state frequency doubling and accessibility of short wavelength in gas HHG in some sense[59]. As shown in Fig. 2d, it employs a resonant-type HHG process in Xenon which reduces the pumping peak power from MW usually used down to KW level. This special VUV laser light source can run at tunable repetition rate between 100 kHz and 10 MHz, provide a photon flux around 2×10^{12} photons/s, and enable ARPES with energy and momentum resolutions better than 2 meV and 0.012 \AA^{-1} , respectively. In particular, with this laser light, the first Brillouin zone of most high temperature superconductors can be accessed, since the photoemitted electron momentum can reach up to 1.2 \AA^{-1} .

3. *Free-Electron Lasers*

Free-electron lasers (FELs) have been recognized as a promising source for the generation of highly brilliant and tunable EUV/X-ray laser radiation, which can be used in the time-resolved photoemission (tr-PES) experiments[60]. FEL does not require a gain medium of gas, liquid or solid like in general lasers. It directly converts the kinetic energy of the relativistic high energy "free" electrons (drawing out of accelerator) into the coherent radiation after such electrons pass through an undulator. In FELs, the electrons are forced to emit coherently by prolonged interaction with the electromagnetic field emitted within the undulator. Depending on the origin of the electromagnetic wave initiating the bunching process, there are two types of FEL operation mechanism: self-amplified spontaneous emission (SASE)[50, 59] and laser seeded mechanism (e.g. high-gain harmonic generation (HGHG), Echo-Enabled Harmonic Generation (EEHG))[51]. In the SASE mechanism like FLASH at DESY, Germany[61], FEL usually shows relatively large shot-to-shot intensity and photon-energy fluctuations and the limited longitudinal coherence. Instead, the laser seeded mechanism like FERMI FEL-1 at Elettra ST, Italy, has the shot-to-shot wavelength stability, low-intensity fluctuations, close to transform-limited bandwidth, transverse and longitudinal coherence and full control of polarization[51, 62]. Besides FLASH and FERMI, there are another two currently operational X-ray FEL facilities: LCLS[63] at SLAC in California, USA, and SACLA[64] at RIKEN in Japan. In addition, some new X-ray FEL facilities are under construction, including the European XFEL[65] at DESY in Germany, the SwissFEL[66] at the Paul Scherrer Institute (PSI) in Switzerland, the PALX-FEL at Pohang Accelerator Laboratory[67] in Korea and the SXFEL[68] at the Shanghai Institute of Applied Physics (SINAP) in China.

To see how a FEL works, in Fig. 7, we show the schematic layout of the first XUV and soft X-ray FEL apparatus FLASH[50, 59, 61]. At the first step, electron bunch patterns are generated by a radio-frequency gun according to the user-preferred operation mode. The electron bunches are compressed longitudinally and accelerated to 1.25 GeV in the linear accelerating structures. Finally they are guided into a long undulator (30 meters) to generate the FEL radiation via the SASE process. At present, FLASH can routinely produce very bright and ultrashort-pulse coherent radiation with a photon energy between 26 and 300 eV, a pulse width of 30–150 fs, a master repetition rate up to 10 Hz (250 kHz single-pulse

repetition rate in the macrobunch mode) and a pulse energy up to 130 μJ .

C. Evaluation of Laser light as a Source for Photoemission

For ARPES, there are basically three types of light sources which have been successfully and routinely used, including rare gas discharge lamps, synchrotron radiation and laser light source. In comparison with discharge lamp and synchrotron radiation, laser light source has many advantages but also some limitations. At current stage, these three light sources are complementary for photoemission experiments.

The earliest photoemission light sources are the noble gas discharge lamps (helium, neon and xenon) with a few discrete photon energies available of 21.2 eV, 40.8 eV, 16.85 eV and 8.5 eV[69–71]. These lamps are compact, practical and particularly affordable to most ARPES labs. A typical example is the modern Helium lamp employing the microwave plasma technique[69]. Such a Helium lamp is still commonly used in many ARPES labs since it can provide rather high flux of 21.2 eV photons to meet the ordinary requirements for ARPES measurements. It is free from space charge effect due to its CW emission nature. However, it has a few obvious shortcomings: insufficient photon flux for high resolution measurements, fixed photon energy, fixed or no polarization, relatively large beam spot size, and leakage of helium gas into the ARPES measurement chamber.

In the last three decades, the continuous advancement of synchrotron technology, especially the emergence of the third generation synchrotron light sources, and the technical progress in two-dimensional detection-type hemispherical electron energy analyzers[72–74] have dramatically improved the performance of ARPES, making it a leading technique for probing electronic structure and many-body interactions in condensed matter physics. The third generation synchrotron sources are featured by very brilliant beam and its continuous tuning in a large photon energy range from VUV to soft-X-ray regions. The beam can be focused to sub-millimeter down to sub-micrometer in size, thus improving the performance of the electron energy analyzer and facilitating ARPES measurements on small or inhomogeneous samples. It has tunable polarizations (linear and circular) that helps to take advantage of the matrix element effects and identify orbital character of the energy bands. Despite the outstanding capabilities of synchrotron-based ARPES, it remains a challenge to achieve a super-high energy resolution better than 1 meV because for synchrotron light

source, the narrow bandwidth is obtained at a cost of photon flux. When the bandwidth reaches 1 meV level, the photon flux usually becomes too low to perform practical ARPES measurements.

The newly developed DUV lasers provide an efficient, compact and low-cost light source for the laboratory-based ARPES systems with many unique advantages[19, 21, 22, 49]. The extremely high and stable photon flux greatly enhances the data acquisition efficiency and data quality. The narrow bandwidth makes it possible to achieve super-high energy resolution in ARPES measurements. In particular, different from synchrotron radiation source, the bandwidth and photon flux of the laser light source are not correlated and can be independently optimized. The utilization of VUV laser light (6.994 eV) has successfully broken the barrier of 1 meV super-high energy resolution that has been a long-sought dream in ARPES technique[21, 22]. In addition, the relatively low photon energy gives rise to high momentum resolution and enhanced bulk sensitivity. It is also easy to control the polarization of the laser light and tune the beam spot size.

Although typical HHG laser light is still hard to achieve high energy resolution in ARPES experiments, recent advances in modified HHG techniques have resulted in laser light at photon energies of 10.5 eV[75] and 11 eV[75, 76]. They have narrow band-width and high photon flux that are comparable to those in solid state UV/VUV laser light. Moreover, for time-resolved photoemission, the laser light with femtosecond-scale pulse width are viable light sources[28–30, 40, 42, 43, 77].

III. DEVELOPMENT OF VUV LASER-BASED ARPES SYSTEMS

A. VUV Laser-Based ARPES with Super-High Energy and Momentum Resolutions

Figure 6 shows a typical VUV-laser based ARPES system. The successful development stems from two major advancements: generation of 6.994 eV VUV laser light and advent of new electron energy analyzer that its angular mode can work properly at a low electron kinetic energy. The new VUV laser-based ARPES system exhibits superior performance, including super-high energy resolution better than 1 meV, high momentum resolution, super-high photon flux, and much enhanced bulk sensitivity[21].

A central part of the system is the picosecond quasi-CW VUV laser light source with a photon energy of 6.994 eV and a bandwidth of ~ 0.26 meV. It is achieved from the SHG using a novel nonlinear optical crystal KBBF (see Fig. 7)[78–80]. A 355 nm commercial frequency-tripled Nd:YVO₄ laser (Vanguard, Spectra Physics) is introduced into the frequency doubling vacuum chamber and focused onto a KBBF crystal by a pair of reflection mirrors and a quartz lens. Here the key element is the optically-contacted KBBF-CaF₂ prism-coupled device where the SHG occurs. The generated 177.3 nm VUV laser light is reflected by two high reflective mirrors and focused by an anti-reflection coated CaF₂ lens onto the sample position in the ARPES analysis chamber. Behind the second reflection mirror, a half-wave plate and a quarter-wave plate working at 177.3 nm are placed for getting linear and circular polarizations of the light. The analysis chamber is isolated in vacuum from the optical chamber by a CaF₂ window; this avoids using complicated differential pumping device to keep the ultra-high vacuum in the analysis chamber.

Compared with 6 eV UV laser light developed for ARPES before[20], the advantage of the 6.994 eV VUV laser light lies in both the superior energy resolution and relatively large momentum space coverage. The linewidth of the VUV laser light source is ~ 0.26 meV which is significantly narrower than ~ 5 meV for the UV laser light[20]. Combined with the resolution of the electron energy analyzer, a high resolution of 0.36 meV have been achieved for the VUV laser-based ARPES[21, 22]. At the photon energy of $h\nu = 6.994$ eV, the maximum in-plane momentum covered is 0.84 \AA^{-1} taking a work function of 4.3 eV while it is 0.67 \AA^{-1} for $h\nu = 6$ eV. The advantage of larger photon energy is obvious here because 6.994 eV laser light can nearly reach the important $(\pi, 0)$ region of high- T_c cuprate superconductors, the iron-based superconductors and many other transition metal oxides.

A natural question that arises when interpreting the laser-based ARPES results is the validity of the so-called sudden approximation, which assumes that the photoelectron leaves the sample before the relaxation of the created photo-hole and neglects the interaction between the outgoing photoelectron and the remaining system[81–83]. For a high photon energy, this is indeed a good approximation as demonstrated in high temperature cuprate superconductors[84]. When the kinetic energy of photoelectron is lower than 3 eV, a typical value for laser-based ARPES, whether the sudden approximation still holds remains to be examined. Koralek et al.[19] directly compared the band dispersions taken at a low photon energy (6 eV) with those at high photon energy and found that the main features are

identical. Their results support the validity of the sudden approximation for laser-based ARPES measurements.

While the VUV laser-based ARPES[20–22] possesses a host of advantages over synchrotron radiation source in terms of energy resolution, momentum resolution, photon flux and bulk sensitivity, it has an obvious drawback in its single photon energy. Due to the photoemission matrix element effects, a single fixed photon energy may make ARPES measurements miss some energy bands and, in the worst case, may not be able to work on some materials. Moreover, for some materials with significant k_z dispersion, different photon energies are necessary to get access to electronic structure at different k_z s. Therefore, the upgrade of laser light source from single photon energy to tunable photon energy is highly necessary in high resolution ARPES community.

The availability of the new NLO crystal, KBBF, provides an opportunity to construct a tunable solid state laser light source for the ARPES technique. Fig. 8 shows the schematic layout of a tunable laser system with a photon energy ranging from 5.9 to 7.1 eV[85, 86]. The tunable Ti:Sapphire laser light (Tsunami ps-version 80 MHz, Spectra Physics) is pumped by a 15 W CW Millennia laser at 532 nm. Its wavelength can be tuned almost continuously from 700 to 850 nm. The pulse duration is 2 ps at 800 nm. The tunable IR beam is first focused inside the BBO-SHG device that is composed of two head-to-head arranged BBO crystals to enhance the SHG output and keep the beam direction during wavelength change. The SHG UV beam is introduced into the frequency doubling vacuum chamber and focused onto KBBF crystal through a quartz window by a reflection mirror and a quartz lens. Then the FHG beam is generated inside the key KBBF-PCT element via a SHG process. The achieved 175 - 212 nm DUV laser light is reflected by two high reflective mirrors and focused by an anti-reflection coated CaF_2 lens onto the sample position in the ARPES analysis chamber. Between the analysis chamber and optical chamber, a CaF_2 window is set to get a vacuum isolation. We note that a similar ARPES system using tunable laser light source was also reported by Kaminski's group[87]. They used a hydrothermally-grown KBBF crystal to realize a tuning of photon energy between 5.3 and 7 eV with a repetition rate of 76 MHz. Although these tunable ARPES can tune the photon energy over a limited energy range, they have proven to be very valuable in ARPES measurements[86, 88, 89].

B. VUV Laser-Based Spin-Resolved ARPES

In order to determine complete electronic states of materials, one needs to have information about all three parameters of electrons, namely, energy, momentum and spin. While ARPES can measure the energy and momentum of electrons, it does not have the spin information. The spin state in materials has become more and more important due to rapid development in both fundamental studies and potential applications, especially for topological quantum state[90, 91] and spintronics[92]. Therefore, a great deal of efforts have been devoted to the development of the spin- and angle-resolved photoemission spectroscopy (SARPES), which combines ARPES with the spin detectors.

Many types of spin detectors have been developed for SARPES by using Mott scattering[93, 94], polarized low-energy electron diffraction (PLEED) from single crystals[95], diffuse scattering[96], and very low energy electron diffraction (VLEED) mechanisms[97]. Among these spin detection schemes, the VLEED spin detector, developed in 1989 for the first time[97], has the highest efficiency due to its higher scattering probability of the low energy electrons ($E_k \sim 6\text{-}10\text{ eV}$) compared with that of Mott scattering ($E_k \sim 20\text{-}100\text{ keV}$). After solving the problem of quick degradation of the ferromagnet target[98], the VLEED spin detector has recently been put into practical use and has achieved nearly two orders of magnitude higher efficiency than that of the conventional Mott detectors[99, 100]. On the other hand, the Mott polarimeters have been proven to be very stable and reliable in operation and therefore are the most widely used spin polarimeters, in spite of its inherent low efficiency (generally ranging from 2×10^{-5} to 1.6×10^{-4}). A lot of progress has been made in improving the efficiency of the retarding Mott polarimeters by adopting good design of retarding optics with large collection solid angle of the scattering electrons. The newly-developed so-called mini Mott polarimeters have efficiency better than 2×10^{-4} that are suitable for developing high-resolution SARPES systems[101–103]. Spin-resolved photoemission system equipped with Mott detectors is usually difficult to achieve high resolution. The energy resolution of spin-resolved ARPES by using Mott detectors was reported to be around 70 meV[101, 102] and has been pushed to be around 8 meV very recently[104]. It is noteworthy that two-dimensional spin detection became available for hemispherical analyzers which drastically increase the spin detection efficiency[105].

The utilization of laser light provides a good opportunity to enhance the performance

of SARPES. The idea is to make use of the extremely high photon flux of laser light to compensate the low efficiency of the Mott spin detector while not losing the overall high energy resolution of the system. This is different from the synchrotron-based SARPES where the increase of photon flux has to be at the sacrifice of the light bandwidth, resulting in a poor energy resolution of 50~100 meV. Based on this idea, a VUV laser-based SARPES with Mott spin detectors was developed in hope of achieving high energy resolution and efficiency.

Figure 9 schematically shows the VUV laser-based SARPES which consists of two major parts: the VUV laser optical system (see Fig. 7) and SARPES system. Two Mott detectors, which are placed perpendicular to each other, are put onto the Scienta–Omicron DA30 analyzer[72] to fulfill the spin- and angle-resolved photoemission measurements. In order to perform ARPES and spin-resolved photoemission measurements at the same time, a portion of photoelectrons passes through two circular spin apertures with adjustable size. Each aperture is connected to a spin transfer lens, and the photoelectrons are transferred to the Mott detectors through the transfer lens for spin-resolved measurements. The photoelectrons are then accelerated electrostatically to 25 keV through the input lens and hit the heavy element Gold (or Thorium) target. The intensity of the scattered electrons are counted by four channeltrons surrounding the target. If the incident photoelectrons are spin polarized, the intensities counted by a pair of channeltrons, for example, left and right channels in the inset of Fig. 9, will be different due to the strong spin-orbital interaction between the incident photoelectrons and the gold (thorium) nucleus in the target. Such an intensity asymmetry from the left and right channels shown in the inset can be used to determine the spin component perpendicular to the scattering plane (paper plane for the inset). Two orthogonal spin components can be determined by one Mott detector with four channels. Two Mott detectors orthogonally placed as shown in Fig. 9 can measure all three orthogonal spin components; one component is measured twice by both Mott detectors that can be used to calibrate the two Mott detectors.

Figure 10 shows the performance of the VUV laser-based SARPES system[47]. Benefiting from the intrinsic narrow linewidth of the VUV laser light (~ 0.26 meV) as well as its super-high photon flux[21], we are able to achieve the best spin-resolved energy resolution of ~ 2.5 meV (Fig. 10c) that is comparable to the best result achieved so far for the spin resolved ARPES measurements (1.7 meV)[106]. Meanwhile the best angular resolution of

our SARPES is around 0.3 degree and the corresponding momentum resolution can be further improved due to the lower photon energy of the VUV laser light ($h\nu=6.994$ eV). There are other outstanding capabilities of the VUV-laser based SARPES system: (1). It is able to do spin- and angle-resolved photoemission measurements simultaneously. This makes it possible to get all three variables of energy, momentum and spin at the same time. In addition, the momentum corresponding to the spin measurement can be determined precisely. (2). It can probe all three spin components of photoelectrons simultaneously. (3). The laser light polarization can be tuned to have different linear or circular polarizations; (4). The utilization of the new DA30 analyzer makes it possible to cover two-dimensional momentum space without rotating the sample. This not only removes the mechanical uncertainty during the sample rotation, but also keeps the same polarization geometry during the SARPES measurements.

The spin-resolving capability of the SARPES was demonstrated by performing simultaneous spin- and angle-resolved measurements on Au(111) surface states[47]. Due to Rashba effects[107, 108], the surface state of Au(111) single crystals splits into two branches with well-defined spin polarization (Fig. 10b)[109, 110]. The spin polarized surface bands form two Fermi surface sheets with well-defined spin textures (Fig. 10a): the inner cone has a left-handed chirality, whereas the outer one has a right-handed chirality[111, 112]. In spin-resolved and angle-resolved mode, the surface band images (Fig. 10e) and spin-resolved energy distribution curves (EDCs) (Fig. 10f) are obtained simultaneously by using the horizontal Mott detector. The band dispersion of the Au(111) surface state in Fig. 10e is measured along the momentum direction depicted as a pink thick line in Fig. 10a. The four spin-resolved EDCs in Fig. 10f are recorded by the four channels of the horizontal Mott detector and correspond to the momentum point highlighted by the dashed blue line in Fig. 10e. Due to much improved energy and angular resolutions, two peaks coming from the two spin polarized surface bands are well resolved in the raw data of the spin-resolved EDCs (Fig. 10f). There is little difference between the two EDCs from the up (U) and down (D) channels, indicating a negligible spin polarization along the Y direction that is an out-of-plane spin component. On the other hand, the two EDCs from the left (L) and right (R) channels show obvious asymmetry in their intensity at two peak positions. Moreover, the relative intensity from these two channels is opposite for the two peaks: for the 0.16 eV binding energy peak associated with the outer cone, the L channel intensity (blue line) is

higher than that of the R channel (red line); for the 0.05 eV peak related with the inner cone, it is reversed. This indicates that there exists spin polarization along the vertical Z axis. The spin directions of the inner and outer cones lie in the plane of the Au(111) surface are opposite. These observations are consistent with previous results on Au(111)[111, 112] and demonstrate the spin-resolving capability of the SARPES system.

C. VUV Laser-Based Time-of-Flight ARPES

In the photoemission process, when light is incident on the sample, electrons are emitted in an entire 2π solid angle. In the first generation of ARPES technique, the electron energy analyzer can only collect electrons emitted along one small solid angle at one time, while the majority of photoelectrons along other angles, although they are already there, are not measured and wasted. The advent of the second generation electron energy analyzer can collect angles along one line in the real space, transforming the ARPES technique from zero-dimension angle coverage to one-dimensional angle coverage. This is a big jump in the ARPES technique because it increases the data acquisition efficiency significantly. The simultaneous collection of multiple angles along one line under the same condition fundamentally changed the game of ARPES. New analysis methods are proposed such as the momentum distribution curves (MDCs)[113], in addition to the usual energy distribution curves (EDCs). This is also a significant step to transform ARPES from a traditional band mapping tool into a probe of many-body effects. However, even in this case, the majority of photoelectrons emitted along other angles are not measured and wasted. It is natural to ask whether it is possible to cover the two-dimensional angle space simultaneously. The latest generation of angle-resolved time-of-flight (ARToF) electron energy analyzer is developed just for realizing this purpose. Many efforts have been put along this direction in the world[48, 75, 86, 114].

A typical ARToF electron energy analyzer (e.g., ARToF 10k from Scienta-Omicron[72]) consists of several cylindrical electrostatic lens and a delay-line detector (DLD), as schematically shown in Fig. 11. When a laser light pulse hits on the sample surface at a time t_0 , electrons emitted within the acceptance angle of the first objective lens are all collected and imaged onto a three-dimensional position sensitive detector placed at the end of the lens set. Electrons with different emission angles will follow different trajectories inside the

lens. When a photoelectron hits the detector, a time t_1 will be recorded. The corresponding kinetic energy of the electron is determined by the time it spends ($t_1 - t_0$) along the particular trajectory. The delay-line detector can measure the position of the electron that hits the detector. The emission angle of the electron can be determined from the location on the DLD because there is a one-to-one correspondence map. In this way, four dimensional data can be collected simultaneously, including the kinetic energy of electrons, the emission direction of the photoelectrons that can be defined by two angles, and the intensity of the photoelectrons.

Two kinds of VUV laser light sources are used for the ARToF-ARPES system. The VUV laser system with a photon energy 6.994 eV follows the similar design of the VUV 6.994 eV laser system used in the laser-based ARPES system that is obtained through SHG of 355 nm photon from the nonlinear optical crystal KBBF[21]. The 355 nm (3.497 eV) 10 ps pumping laser light pulse comes from a Nd:YVO₄ laser light source. It is focused onto the KBBF-PCT device inside the frequency doubling chamber. After frequency doubling process, the diffused 177.3 nm (6.994 eV) VUV laser light is focused onto the sample position in the ARPES measurement chamber. The beam size is tunable by choosing different focus lens. Different photon polarizations (linear and circular) can be achieved with a half wave plate and a quarter wave plate. The main difference between this 6.994 eV laser system with the previous one used in laser ARPES system[21] is that the laser light source has a low repetition rate between 0.2 MHz and 1 MHz. Another VUV laser light source with a photon energy 10.897 eV is equipped which is based on the non-linear optical sum-frequency conversion process[115].

There are a number of advantages in the VUV laser-based ARToF-ARPES system. First, it measures two-dimensional momentum space simultaneously. Compared with the regular hemisphere analyzer that measures one line of momentum, the efficiency of momentum coverage is increased by more than 2 orders of magnitude. Like the jump from the first generation one-angle-at-one-time to the second generation of one-line-at-a-time, this jump to the third generation of one-area-at-a-time will bring about a fundamental change of the ARPES technique. It makes it possible to observe the Fermi surface in real time that is impossible before. Since the two-dimensional angles are measured under the same condition, it will help to reveal fine electronic structure that are hard to resolve before. Second, the VUV laser-based ARToF-ARPES has high energy and momentum resolutions. Third, the

time-of-flight analyzer counts the number of electrons hitting the detector; this is different from the usual hemisphere analyzer where the photoelectron signal is first converted to photon signal by using a phosphor and then the intensity of the photons is recorded by a CCD camera. The ARToF-ARPES measurements can give a low background, and suppress the signal nonlinearity effect that is usually encountered in a hemisphere analyzer.

To demonstrate the performance of the VUV laser ARToF-ARPES system, Fig. 12a shows the Fermi edge of a polycrystalline Au sample, measured with the 6.994 eV laser light at a low temperature of ~ 9.5 K which gives a Fermi edge width of 3.37 meV. After subtracting the temperature broadening, the overall instrumental energy resolution of the 6.994 eV laser ARToF-ARPES system is better than 1 meV. In Fig. 12(b-e), the space charge effect was tested using the same polycrystalline Au measured with different powers and repetition rates of the laser light. An obvious space charge effect was observed when 0.1 mm spot size and 200 kHz were used (Fig. 12b). When the repetition rate was increased up to ~ 1 MHz, the space charge effect became nearly absent (Fig. 12c). Fig. 13 shows the 6.994 eV laser-based ARToF-ARPES measurements on an optimally-doped $\text{Bi}_2\text{Sr}_2\text{CaCu}_2\text{O}_{8+\delta}$ (Bi2212) superconductor measured at 15 K and Fig. 13a is the measured Fermi surface. Due to the data continuity in the covered momentum space, one can extract high-quality band structure along any momentum cut (Fig. 13(f-j)). Such a capability of the data analysis is hard to be realized in the regular ARPES based on the hemispherical energy analyzer. Non-linearity effect is examined by taking the ARPES measurements at a low count rate (Fig. 13b) and a high count rate (Fig. 13c) along the same momentum cut following a proposed procedure[116]. The result indicates that there is nearly no nonlinearity effect in the ARToF-ARPES system (Fig. 13d). This is further confirmed by the same lineshape of two photoemission spectra measured using different count rate (Fig. 13e).

D. Laser-Based Time-Resolved ARPES

Ultrafast dynamics in solids, such as the photo-induced phase transitions[117–123], photo-induced hidden phases or photo-enhanced density wave orders[124–126], and especially the photo-induced possible superconductivity[127–129], have attracted broad attention in condensed matter physics. In these ultrafast studies, ultrashort infrared laser light pulses, far infrared laser light pulses or even THz radiations are generally used as the pump source

to create non-equilibrium states in materials. The photon source is commonly used as the probe because it is relatively easy to achieve ultrashort pulses (femtoseconds) to study the dynamics of electronic structure. The recently-developed femtosecond electron pulses from accelerators[130] and ultrashort X-ray pulses from free-electron lasers[131] bring new opportunities in probing the dynamics of the motion of atoms in real space. Among all the ultrafast probing techniques, the time-resolved ARPES (tr-ARPES) has opened a new window into directly probing the electronic dynamics in superconductors[132–139], topological insulators[114, 140–142], density wave systems[29–31, 56, 143], and other strongly correlated systems[144–148].

In a tr-ARPES system, as schematically shown in Fig. 14a, an infrared pump laser light pulse drives the sample into a non-equilibrium state. Subsequently, an ultraviolet laser light is used to probe the electrons which are usually captured by an electron energy analyzer in an ARPES setup. The time resolution is achieved by varying the delay time between the pump and probe pulses. For $t < 0$, the probe pulse arrives before the pump pulse, and thus corresponding to an equilibrium measurement. For $t > 0$, the probe pulse arrives after the pump pulse, and hence corresponding to a non-equilibrium measurement.

In tr-ARPES experiments, infrared laser light pulses (Ti: sapphire laser) are usually used as the pump, far infrared laser light pulses are used in a few experiments, and so far there is no report of THz radiation used as the pump yet. The tunability of the pump photon energy in the time-resolved ARPES is limited by the low energy conversion efficiency in the non-linear process in far infrared range.

In tr-ARPES experiments, high repetition rate of the probe pulse is necessary in order to photoemit reasonable number of electrons and, at the same time, to reduce the space charge effect for achieving a reasonably high energy resolution. According to the generation mechanism, the probe photon sources in tr-ARPES can be divided into three classes. The first is from the frequency conversion in non-linear crystals, and the wavelength is in the ultraviolet range with a photon energy usually no higher than 7 eV. The tr-ARPES setup based on such a solid laser system is adapted by many groups because of the advantages of low cost, high stability, high energy resolution and easy operation, although there is a limitation on the accessible momentum space of a material[38, 40, 77, 114, 139, 149]. A typical schematic of such a setup is shown in Fig. 14b. Laser light pulses are generated using a mode-locked Ti:sapphire oscillator with center wavelength around 836 nm. Two

separated BBO nonlinear crystals are used to double the frequency of the output beam from the oscillator twice, achieving ultrashort ultraviolet probe pulses with a centre wavelength around 209 nm. The other branch of the beam (839 nm) directly outputted from the laser oscillator is used as the pump. The two beams are focused precisely at the same point on the sample in the ARPES chamber. Time resolution is achieved by precisely varying the optical path length of the pump beam using a fine linear translation stage. The overall time resolution of such setups can be better than 100 fs and the corresponding energy resolution is around 20 meV.

The second class of the probe source in the tr-ARPES is based on HHG process in gas phases, which are usually used to produce ultrashort laser light pulse with much shorter wavelength and shorter pulse length[24, 43–45, 56, 150–153]. In addition to the broad bandwidth in frequency of the probe pulses due to the Fourier transfer limit, the low repetition rate of such a system also induces strong space charge effect, making it difficult to measure samples with a high energy resolution. Recently, a high repetition rate (250 kHz) HHG system was developed in tr-ARPES experiment, but it has a very low probe photon flux because of the low three-order harmonic generation efficiency[154]. The third class of the probe source in the tr-ARPES is new and is under development in conjunction with free-electron laser sources[59, 155, 156]. Such laser source will have advantages of variable probe photon energy and pulse duration. However, at present, this technique is limited by the low repetition rate of the pulses and poor energy resolution.

IV. SCIENTIFIC APPLICATIONS OF LASER-BASED ARPES SYSTEMS

A. New Coupling Mode and Extraction of the Eliashberg Functions

The dramatic improvement of the ARPES technique has transformed it from a usual band mapping tool into a probe on the many-body effects in materials[13]. This is particularly important for understanding the anomalous normal state properties and the superconductivity mechanism of the high-temperature cuprate superconductors. The first indication of many-body effects in cuprates was observed in ARPES measurements on Bi2212 where a dispersion kink is identified along the nodal direction[157–161]. This was made possible mainly due to the advent of the second generation electron energy analyzer that can mea-

sure multiple angles along a line simultaneously. Since the many-body effects are subtle and hard to detect, high resolution and high data statistics are required in the ARPES measurements. This is particularly important when quantitative analysis of the many-body effects are performed[33, 162].

The development of VUV laser-based ARPES with superior energy and momentum resolutions, as well as high data statistics due to high photon flux, provides a powerful tool to investigate the many-body effects in materials. Fig. 15 shows one example to demonstrate the power of the laser-based ARPES on this issue which studied the nodal band renormalization in a Bi2212 superconductor[163]. The original high precision ARPES data is shown in Fig. 15a and quantitative dispersion relation and the scattering rate are shown in Fig. 15b. Fig. 15c shows the effective real part of the electron self-energy at different measurement temperatures. In addition to the well-known 70 meV mode-like feature that shows up very clearly in the measurements, there are new features emerging at high energies: a dip-like feature at ~ 115 meV and a hump structure at ~ 150 meV, which are not resolved before. They are only present in the superconducting state and their amplitude gets stronger with decreasing temperature. Since the energy scale of phonons in Bi2212 is below 100 meV[164], these new energy scales are unlikely due to electron coupling with phonons; some new mode couplings may exist in the superconducting state of Bi2212[165–167].

One of the big challenges in the study of high-temperature superconductors is to understand the superconductivity mechanism. One critical issue concerns how the electrons interact and form Cooper pairs. In the conventional superconductors, it was proposed by the BCS theory of superconductivity that the electron pairing is mediated by exchanging phonons. The experimental validation of the BCS theory in the conventional superconductors is realized by the tunneling experiment[168] and the subsequent elegant analyses[169]. The pairing Eliashberg function extracted from the tunneling data of Pb by direct inversion of the gap function exhibits a striking similarity to the phonon density of states measured directly from neutron scattering. This provided a compelling evidence that the electrons in Pb form Cooper pairs by exchanging phonons. It is natural to ask whether similar approach can be used in high temperature cuprate superconductors. This turns out to be unfeasible because high T_c superconductors show a d -wave superconducting order parameter that is different from the s-wave case in conventional superconductors like Pb. In this case, experimental tools that have momentum resolution have to be employed and ARPES turned out

to be a promising technique to address the issues[170]. Although the idea has been around since 2003, no attempts have been successful because extremely high precision ARPES measurements are necessary for such analyses, and for a long time no ARPES data can satisfy such a demanding requirement.

The development of the VUV laser-ARPES provides an opportunity to address the important issue of pairing mechanism in high temperature cuprate superconductors by extracting the pairing Eliashberg functions in the superconducting state[171]. Since the pairing self-energy, and then the pairing Eliashberg function, are obtained from the signal difference between the superconducting state and the normal state, measurements of such a weak superconductivity-induced effect require high data precision (better than 1%), in addition to high energy and momentum resolutions. Such a stringent demand is recently met in the VUV laser-based ARPES, the related results are summarized in Fig. 16. From high resolution ARPES data measured below T_c (Fig. 16a) and above T_c (Fig. 16b), with the analysis of superconducting Green's functions, the normal self-energy Σ (Fig. 16c) and pairing self-energy ϕ (Fig. 16d and e) are successfully extracted. By direct inversion of the Eliashberg equations, the normal Eliashberg function (\mathcal{E}_N) and pairing Eliashberg function (\mathcal{P}_N) are extracted (Fig. 16). The extracted pairing Eliashberg function shows a peak at ~ 50 meV, a flat featureless region extending to high energy, and a cut-off at high energy depending on the location of the momentum cuts. This is the first time that the normal Eliashberg function and the pairing Eliashberg function are extracted from ARPES measurements. They provide critical information on examining various theoretical models for understanding high-temperature superconductivity[172].

B. Direct Observation of Spin-Orbital Locking in Topological Insulators

Topological insulators have attracted much attention because of their unique electronic structure and spin texture, as well as their novel physical properties[90, 91]. In its metallic surface state with helical spin texture, the electron spin is locked to its crystal momentum[90, 91]. Theoretical calculations also predict that the spin texture might be coupled with the orbital texture in topological insulators[173]. Such a new spin-orbital texture, if proved experimentally, can provide new insight on the spin texture of topological insulators and paves a way for light manipulation on spin textures in topological insulators. To directly

prove the possible spin-orbital locking in topological insulators, it is suggested that high resolution spin-resolved ARPES must be used. In addition, the light must have tunable polarizations[173].

The VUV laser-based SARPES system can meet all the requirements for examining the spin-orbital locking in topological insulators[47]. In order to do orbital-selective SARPES measurements, different linear polarization states of the incident VUV laser light with *s*- or *p*-polarization geometries were set and different orbital textures of the Bi₂Se₃ Dirac surface state were observed by taking advantage of the photoemission matrix element effects. The orbital textures of the Dirac cone detected under *s*- and *p*-polarization geometries are schematically shown in Fig. 17e and f, respectively. The spin texture of the topological surface state of Bi₂Se₃ under different polarization geometries were further measured, as shown in Fig. 17, which contains both the band mapping of the topological surface states (Fig. 17c and d) and the spin-resolved photoemission spectra (Fig. 17a and b). The spin-resolved photoemission spectra (energy distribution curves, EDCs) in Fig. 17a are measured under the *s* polarization geometry at five representative momentum points along the $\bar{\Gamma}\bar{K}$ cut as marked by the dashed lines in the band image measured from regular ARPES (Fig. 17c). Likewise, spin-resolved EDCs in Fig. 17b with the *p* polarization geometry are measured on five momentum points along the $\bar{\Gamma}\bar{K}$ cut as marked by the dashed lines in the band image in Fig. 17d. At a given momentum point, the two EDCs represent the in-plane (sample surface plane) spin component along the vertical Z direction with up (red line plus circles) and down (blue line plus triangles) spin orientation (for definition of the spin direction, see Fig. 10d). By systematic observation of the momentum-dependent spin polarization of the Dirac cone in *s*- and *p*-polarization geometries, the spin texture is determined and the relationship between the spin and orbital textures is revealed, as summarized schematically in Fig. 17e and f. The spin textures observed in *s*- and *p*-polarization geometries are different. In particular, for *s*-polarization geometry, the upper Dirac cone and lower Dirac cone share the same chirality, which is distinct from the usual observation of spin texture in the topological surface state. On the other hand, in *p*-polarization geometry, the spin textures of the upper Dirac cone and lower one show opposite chirality, which is consistent with the total spin texture of the topological surface state. By switching the incident laser light from *p*- to *s*-polarization geometry, the spin texture for the upper Dirac cone changes from the left-handed to the right-handed chirality while it keeps the same for the lower Dirac cone.

These observations cannot be explained by the usual spin picture in topological insulators, but are fully consistent with the predictions in terms of the spin-orbital locking. These results thus provide a strong experimental evidence for the orbital-selective spin texture in the Bi_2Se_3 topological insulator[47].

C. Novel Electronic Structure of WTe_2 and ZrTe_5 Revealed by VUV Laser-Based ARToF-ARPES

1. Complete electronic structure and topological nature of WTe_2

WTe_2 has been well-known for its manifestation of extremely large magnetoresistance that is proposed to be due to the compensation of electrons and holes in the material[174]. A complete understanding of its electronic structure is a prerequisite to pin down the origin of the anomalous transport properties. However, due to the existence of multiple pockets in a limited momentum space, the full electronic structure of WTe_2 remains controversial. Lately, WTe_2 has ignited another surge of excitement because it is theoretically predicted to be the first material candidate that may realize type-II Weyl state[175]. However, experimental evidence on the identification of type II Weyl Fermions in WTe_2 is still lacking.

Taking advantage of the VUV laser-based ARToF-ARPES system with superior instrumental resolution, a complete picture of the electronic structure of WTe_2 has been resolved[48]. Fig. 18 shows the measured Fermi surface of WTe_2 where the existence of a surface state is clearly identified. High temperature ARPES measurements make it possible to reveal electronic states above the Fermi level where the Weyl points are predicted to be located. The observed connection of the surface state with the bulk bands, its momentum evolution, its momentum and energy locations, are all in good agreement with the calculated band structure. These results provide electronic signatures that are consistent with the type II Weyl state in WTe_2 although further efforts are needed to fully prove the realization of type II Weyl state in WTe_2 . The first-time complete electronic structure of WTe_2 , including all the Fermi pockets and near- E_F energy bands also makes it possible to determine accurately the electron and hole concentrations and their temperature dependence[176]. With increasing temperature, the overall electron concentration increases while the total hole concentration decreases. It indicates that, the electron-hole compensation, if exists, can

only occur in a narrow temperature range and in most of the temperature range there is an electron-hole imbalance. These results are not consistent with the perfect electron-hole compensation picture that is commonly considered to be the cause of the unusual magnetoresistance in WTe_2 . They provide new insight on understanding the origin of the unusual magnetoresistance in WTe_2 [48, 176].

2. *Temperature-Induced Lifshitz Transition and Topological Nature in ZrTe_5*

The topological materials have attracted much attention recently for their unique electronic structure, spin texture and peculiar physical properties. While three-dimensional topological insulators are becoming abundant, two-dimensional topological insulators remain rare, particularly in natural materials. ZrTe_5 has host a long-standing puzzle on its anomalous transport properties manifested by its unusual resistivity peak and a sign reversal of the Hall coefficient and thermopower; the underlying origin remaining elusive. Lately, ZrTe_5 has ignited renewed interest because it is predicted that single-layer ZrTe_5 is a two-dimensional topological insulator and there is possibly a topological phase transition in bulk ZrTe_5 [177]. However, the topological nature of ZrTe_5 remains under a heated debate.

By using the VUV laser-based ARToF-ARPES system, high-resolution ARPES measurements are performed on the electronic structure and its detailed temperature evolution of ZrTe_5 [86]. As displayed in Fig. 19, the electronic property of ZrTe_5 is dominated by two branches of nearly-linear dispersion bands with a gap between them at the Brillouin zone center. The overall electronic structure exhibits a dramatic temperature dependence; it evolves from a p-type semimetal with a hole-like Fermi pocket at high temperature, to a semiconductor around ~ 135 K where its resistivity exhibits a peak, to an n-type semimetal with an electron-like Fermi pocket at low temperature. These results provide direct electronic evidence on the temperature-induced Lifshitz transition in ZrTe_5 , and a natural understanding on the underlying origin of the transport anomaly at ~ 135 K. In addition, one-dimensional-like electronic features are observed from the edges of the cracked ZrTe_5 samples implying that ZrTe_5 is a weak topological insulator[86].

D. Time-Resolved ARPES on High-Temperature Cuprate Superconductors and Topological Insulators

Time-resolved ARPES has been widely used in studying the momentum-resolved electronic dynamics in high-temperature superconductors, topological insulators, density wave systems, and other strongly-correlated systems. After photon excitation, the electron-boson coupling, specific mode vibration, the superconducting gap, and so on can be tracked by tr-ARPES. Here we highlight two applications of tr-ARPES in the study of ultrafast electronic dynamics in the high-temperature superconductors and topological insulators.

It remains unclear how electrons bind into Cooper pairs in high-temperature cuprate superconductor and what the origin of the abnormal pseudogap phase is in the underdoped region. Tr-ARPES provides a unique approach to probe the non-equilibrium quasi-particle dynamics[132, 133, 139, 178], non-equilibrium phase diagram[179], many-body problem[137, 138], energy gap dynamics[180], and so on. The many-body interactions is important in understanding the superconductivity mechanism. Tr-ARPES has the capabilities of tracking the electron-boson interaction dynamics and the non-equilibrium superconducting gap simultaneously, providing information to clarify the role of electron-boson coupling in generating superconductivity.

Figure 20 shows an example of such a study along this direction[137]. In the optimally-doped Bi2212, the nodal kink around 70 meV signifies electrons coupled with some bosons at this energy scale. Far below the superconducting transition temperature T_c , intense ultrashort laser light pulse weakens the kink strength apparently (Figs. 20a and b). This can be further confirmed by the extracted effective real part of the electron self-energy shown in the lower panel of Fig. 20c. By simultaneously tracking the superconducting energy gap, it is found that the photo-induced change of the electron-boson coupling strength is proportional to the change of the superconducting energy gap, while above T_c when the superconducting gap fully closes, pumping photons has a negligible effect on the kink (upper panel in Fig. 20c). Similar negligible photo-induced change of the kink structure is also observed in the normal state of a heavily overdoped Bi2201 sample at very low temperature[137]. These findings establish a strong correlation between the nodal electron-boson coupling and the superconductivity in high temperature cuprate superconductors, and demonstrate that tr-ARPES is an emerging powerful tool to address non-equilibrium self-energy dynamics and

many-body interactions in materials.

In topological insulators, such as Bi_2Se_3 , there is no direct electron-hole recombination because of the opposite spin texture at the same momentum in the Dirac dispersion. It is therefore necessary to use momentum-resolved technique, such as tr-ARPES, to study the manipulation of the exotic surface states by ultrashort laser light pulse[41, 114, 181, 182].

When moving in a periodic potential (crystal lattice), electrons' energy locks on to their momentum periodically in a parabolic form and are gapped at the boundary of the Brillouin zone; this is named Bloch states. Under an intense electromagnetic field (usually can be created by an ultrashort intense laser light pulse), electrons move in solids periodically in both space and time, and this is called Floquet-Bloch states. When pumping Bi_2Se_3 with linear polarized laser light pulses, the periodic duplication of dispersion in energy is demonstrated by tr-ARPES as shown in Fig. 21a. The energy gap can be resolved at the band crosses away from the Dirac point (Figs. 21b and c). Further studies show that using circular polarized laser light pulse, a gapped Dirac cone can be observed, indicating the broken time-reversal symmetry induced by ultrashort laser light pulse. These observations provide strong evidence of the Floquet-Bloch bands in solids and pave the way for optical manipulation of quantum states in matter[181].

Except for the novel study in optical control of the topological surface states, the non-equilibrium quasiparticle dynamics induced by ultrashort laser light pulses in topological insulators can also be tracked by tr-ARPES. Fig. 21d shows the non-equilibrium quasiparticle oscillations in both bulk and surface electronic states which are apparently different from each other. This indicates that there are different mechanisms in controlling the dynamics of photo-induced non-equilibrium quasiparticles in bulk and surface electronic states. Results of Fourier transforms confirm the observations and reveal an additional vibration mode at 2.05 THz only in the surface states, while in both the bulk and surface states there is another mode at a higher frequency (2.23 THz) (Fig. 21(e)). The 2.23 THz vibration is attributed to an A_{1g} phonon mode and the 2.05 THz vibration is due to the termination of the crystal and thus reduction of the interlayer van der Waals forces, which serve as restorative forces for out-of-plane lattice distortions[142]. The study showcases the power of tr-ARPES to resolve distinct modes coupling to individual bands.

V. OUTLOOK AND PERSPECTIVE

ARPES has played a key role in studying the novel quantum materials in condensed matter physics. There is no doubt that it will continue to play a leading role in the years to come. Many prominent physics problems ask for further improvement of the ARPES capabilities. The emergence of laser-ARPES in the last ten years has created a new path for endowing ARPES with unique and superior performances. It has already demonstrated its power in studying quantum materials like high temperature superconductors and topological materials. There is still plenty of room for laser-ARPES to further enhance its capabilities. We will expect its continuous improvement along the following directions:

1. Laser light sources with higher photon energy, narrower bandwidth, and shorter pulse duration.

As we have seen, the laser photon energy for high-resolution ARPES has steadily increased from 6 eV, to 7 eV, to 11 eV in the last ten years. To cover a large momentum space, it is important to further increase the laser photon energy, while keeping its unique characteristics like narrow bandwidth and extremely high photon flux. There have been big efforts along this direction. High order harmonic generation is a promising approach to get higher laser photon energy, and further work is needed to increase its repetition rate and average power in order to be used for high resolution ARPES.

There is still room to further improve the energy resolution of the ARPES technique. For example, measurement of the superconducting gap in superconductors with lower T_c such as Sr_2RuO_4 with a T_c at ~ 1 K and CeCoIn_5 with a T_c at 2.3 K definitely requires an energy resolution much better than 1 meV. Next generation ARPES should improve the best energy resolution from 1 meV to the order of μeV . This requires laser light sources to have much narrower bandwidth. Since photoemission process is closely related to the space charge effect that may deteriorate the energy resolution, the ultimate energy resolution may be limited by the space charge effect, which becomes particularly serious in laser-ARPES because of laser light's high photon flux and relatively small beam size. To overcome the space charge effect, it is desirable to increase the repetition rate of the laser light sources in order to reduce the number of photons in one pulse. Development of continuous-wave laser light will be most ideal because in principle it does not produce space charge effect[37, 55, 183]. The continuous-wave laser light may become particularly useful for spin-resolved ARPES where

high photon flux is necessary in order to compensate the low efficiency of spin detectors which will inevitably causes strong space charge effect if it is a pulsed laser light source.

Spatially-resolved ARPES will play an important role in studying inhomogeneous systems. Focusing laser light to microns or sub-microns will be beneficial to perform spatially-resolved ARPES. For materials that are spatially inhomogeneous or new materials that are hard to get big enough single crystals, in order to detect their intrinsic electronic structure, spatially-resolved ARPES is necessary. With the micron-scale or even nanoscale spot size, spatially-resolved ARPES will play an irreplaceable role in obtaining information about phase separation or multiple domains of materials.

Tunable laser light source that can cover a large range of photon energy needs to be developed. This is helpful in dealing with the photoemission matrix element effects and increasing the variety of materials that can be measured. Furthermore, tunable laser light is very important for measuring materials with strong three-dimensionality of electronic structure.

Time-resolved ARPES is a powerful tool for investigating electron dynamics and non-equilibrium state. For strongly correlated systems, such as high temperature superconductors, electronic dynamics happens with an energy scale on the order of meV and a time scale of femtosecond. The development of laser light source that can produce very short pulse and high energy resolution will promote time-resolved ARPES applications. High repetition rate, relatively narrow bandwidth, and tunability of the probe pulse are important in time-resolved ARPES studies. Also in future time-resolved APRES, developing strong tunable pump pulses from violet to far infrared, even to THz range, which can be used to coherently excite the low energy modes such as the lattice vibrations in materials, will be important in controlling the electronic structure in materials by strong laser light pulses.

With the fast development of free electron lasers, and considering their extremely high photo flux, ultrashort pulse width and spatial and temporal coherence, their extensive applications in photoemission is highly expected. Currently, the time-resolved photoemission experiments using free electron lasers face challenges of very strong space charge effect, poor energy resolution and insufficient statistics due to very low repetition rate and too high pulse intensity. These issues can be addressed by significantly increasing the repetition rate up to ~ 100 kHz - \sim MHz and manipulating the photon pulse energy and bandwidth. In this regard, LCLS-II and European XFEL employing superconducting RF accelerators may

provide some unique opportunities in time-resolved photoemission techniques.

2. Improvement of the photoelectron detection technique

We have seen the dramatic improvement of the electron energy analyzer from the first generation to measure one angle at one time, to the second generation to measure multiple angles along one line, to the present third generation to measure a two-dimensional area of angles. The detection of photoelectrons covering full 2π solid angle at one time is ideal. The technique is under development and should be implemented in all the electron energy analyzers in the future. In the mean time, the energy resolution has also been improved from 10 meV to 1 meV to nowadays 0.1 meV. Further increase of the energy resolution of the ARPES system to μeV level asks the analyzers to have even better energy resolution. In the spin-resolved ARPES technique, concurrent detection of spin state during the simultaneous ARPES measurement of the two-dimensional momentum space represents a future direction to develop.

3. Improvement of the sample environment

The utilization of laser light source in ARPES has resulted in super-high energy resolution better than 1 meV[21, 22]. However, the sample temperature will also cause spectral broadening. For most of ARPES systems at work, the lowest sample temperature is usually about 10 K which corresponds to about 3.7 meV Fermi broadening. This is significantly larger than 0.26 meV bandwidth of the VUV laser light source. To take full advantage of the super-high energy resolution of laser-ARPES, it is imperative to lower the sample temperature to below 1 K or even lower. Ultra-low sample temperature is also necessary for studying materials with low temperature scales, like superconductors with low T_c . Efforts have been put into developing new cryostats with ultra-low temperature[184]. A VUV laser-based ARPES system with ultra-low sample temperature (below 1 K) has been developed in the institute of physics, Beijing[185].

4. Combination of ARPES with other techniques

For some deep physics problems, one needs to get information about various aspects in order to have a complete picture. Therefore, integration of various photoemission techniques, such as angle-resolved photoemission, spin-resolved photoemission, spatially-resolved photoemission, and time-resolved photoemission, in one system is a good option. Also ARPES can be integrated with other techniques such as structural analysis tools to obtain both electronic structure and lattice and magnetic structures simultaneously. Last but not least,

because ARPES can only work on a clean and flat surface, it becomes very fruitful to integrate sample preparation into the ARPES system. Combining ARPES with *in situ* sample preparation like molecular beam epitaxy (MBE) and *in situ* sample characterization like scanning tunneling microscope (STM) has produced significant results and will become popular in the future.

With further development of laser-ARPES and its related techniques, we believe it will play more and more important role in studying novel quantum materials in the near future.

-
- [1] H. Hertz. Ueber Einen Einfluss Des Ultravioletten Lichtes auf Die Electriche Entladung. *Ann. Phys. (Leipzig)*, 17:983, 1887.
 - [2] A. Einstein. Generation and Conversion of Light with Regard to a Heuristic Point of View. *Annalen Der Physik*, 17(6):132–148, 1905.
 - [3] C. Nordling, E. Sokolowski, and K. Siegbahn. Precision Method for Obtaining Absolute Values of Atomic Binding Energies. *Physical Review*, 105(5):1676–1677, 1957.
 - [4] N. V. Smith and M. M. Traum. Angular Dependence of Photoemission from the 110 Face of GaAs. *Physical Review Letters*, 31(20):1247–1250, 1973.
 - [5] N. V. Smith, M. M. Traum, and F. J. DiSalvo. Mapping Energy-Bands in Layer Compounds from Angular-Dependence of Ultraviolet Photoemission. *Solid State Communications*, 15(2):211–214, 1974.
 - [6] S. Hüfner. *Photoelectron Spectroscopy*. Springer, Berlin, 2003.
 - [7] A. A. Abrikosov, L. P. Gorkov, and I. E. Dzialoshinskii. Quantum Field Theoretical Methods in Statistical Physics, Pergamon, Elmsford. 1965.
 - [8] L. Hedin. Solid State Physics: Advances in Research and Applications, Academic, New York. 1969.
 - [9] G. D. Mahan. Quantum Theory of Many-Particle Systems, Plenum, New York. 1981.
 - [10] G. Rickayzen. Green’s Functions and Condensed Matter in Techniques of Physics, Academic, London. 7, 1991.
 - [11] A. Damascelli, Z. Hussain, and Z. X. Shen. Angle-Resolved Photoemission Studies of the Cuprate Superconductors. *Reviews of Modern Physics*, 75(2):473–541, 2003.
 - [12] J. C. Campuzano, M. R. Norman, and M. Randeria. In the Physics of Superconductors,

- edited by K. H. Bennemann and J. B. Ketterson (Springer, New York, 2004), Vol. 2.
- [13] X. J. Zhou, T. Cuk, T. Devereaux, N. Nagaosa, and Z.-X. Shen. Angle-Resolved Photoemission Spectroscopy on Electronic Structure and ElectronPhonon Coupling in Cuprate Superconductors, edited by J. R. Schrieffer (Springer, New York, 2007).
 - [14] G. Beamson, D. Briggs, S. F. Davies, I. W. Fletcher, D. T. Clark, J. Howard, U. Gelius, B. Wannberg, and P. Balzer. Performance and Application of the Scienta ESCA300 Spectrometer. *Surface and Interface Analysis*, 15(9):541–549, 1990.
 - [15] N. Martensson, P. Baltzer, P. A. Bruhwiler, J. O. Forsell, A. Nilsson, A. Stenborg, and B. Wannberg. A Very High-Resolution Electron Spectrometer. *Journal of Electron Spectroscopy and Related Phenomena*, 70(2):117–128, 1994.
 - [16] Y. Maeno, H. Hashimoto, K. Yoshida, S. Nishizaki, T. Fujita, J. G. Bednorz, and F. Lichtenberg. Superconductivity in a Layered Perovskite without Copper. *Nature*, 372(6506):532–534, 1994.
 - [17] C. Petrovic, P. G. Pagliuso, M. F. Hundley, R. Movshovich, J. L. Sarrao, J. D. Thompson, Z. Fisk, and P. Monthoux. Heavy-Fermion Superconductivity in CeCoIn₅ at 2.3 K. *Journal of Physics: Condensed Matter*, 13(17):L337, 2001.
 - [18] T. Kiss, F. Kanetaka, T. Yokoya, T. Shimojima, K. Kanai, S. Shin, Y. Onuki, T. Togashi, C. Zhang, C. T. Chen, and S. Watanabe. Photoemission Spectroscopic Evidence of Gap Anisotropy in an f-Electron Superconductor. *Physical Review Letters*, 94(5):057001, 2005.
 - [19] J. D. Koralek, J. F. Douglas, N. C. Plumb, Z. Sun, A. V. Fedorov, M. M. Murnane, H. C. Kapteyn, S. T. Cundiff, Y. Aiura, K. Oka, H. Eisaki, and D. S. Dessau. Laser Based Angle-Resolved Photoemission, the Sudden Approximation, and Quasiparticle-Like Spectral Peaks in Bi₂Sr₂CaCu₂O_{8+δ}. *Physical Review Letters*, 96(1):017005, 2006.
 - [20] J. D. Koralek, J. F. Douglas, N. C. Plumb, J. D. Griffith, S. T. Cundiff, H. C. Kapteyn, M. M. Murnane, and D. S. Dessau. Experimental Setup for Low-Energy Laser-Based Angle Resolved Photoemission Spectroscopy. *Review of Scientific Instruments*, 78(5):053905, 2007.
 - [21] G. D. Liu, G. L. Wang, Y. Zhu, H. B. Zhang, G. C. Zhang, X. Y. Wang, Y. Zhou, W. T. Zhang, H. Y. Liu, L. Zhao, J. Q. Meng, X. L. Dong, C. T. Chen, Z. Y. Xu, and X. J. Zhou. Development of a Vacuum Ultraviolet Laser-Based Angle-Resolved Photoemission System with a Superhigh Energy Resolution Better than 1 meV. *Review of Scientific Instruments*, 79(2):023105, 2008.

- [22] T. Kiss, T. Shimojima, K. Ishizaka, A. Chainani, T. Togashi, T. Kanai, X. Y. Wang, C. T. Chen, S. Watanabe, and S. Shin. A Versatile System for Ultrahigh Resolution, Low Temperature, and Polarization Dependent Laser-Angle-Resolved Photoemission Spectroscopy. *Review of Scientific Instruments*, 79(2):023106, 2008.
- [23] H. S. Karlsson, G. Chiaia, and U. O. Karlsson. System for Time- and Angle-Resolved Photoelectron Spectroscopy Based on an Amplified Femtosecond Titanium:Sapphire Laser System. *Review of Scientific Instruments*, 67(10):3610–3615, 1996.
- [24] S. Mathias, L. Miaja-Avila, M. M. Murnane, H. Kapteyn, M. Aeschlimann, and M. Bauer. Angle-Resolved Photoemission Spectroscopy with a Femtosecond High Harmonic Light Source Using a Two-Dimensional Imaging Electron Analyzer. *Review of Scientific Instruments*, 78(8):6465, 2007.
- [25] R. Haight, J. A. Silberman, and M. I. Lillie. Novel System for Picosecond Photoemission Spectroscopy. *Review of Scientific Instruments*, 59(9):1941–1946, 1988.
- [26] W. Nessler, S. Ogawa, H. Nagano, H. Petek, J. Shimoyama, Y. Nakayama, and K. Kishio. Femtosecond Time-Resolved Study of the Energy and Temperature Dependence of Hot-Electron Lifetimes in $\text{Bi}_2\text{Sr}_2\text{CaCu}_2\text{O}_{8+\delta}$. *Physical Review Letters*, 81(20):4480–4483, 1998.
- [27] R. Haight and D. R. Peale. Tunable Photoemission with Harmonics of Subpicosecond Lasers. *Review of Scientific Instruments*, 65(6):1853–1857, 1994.
- [28] L. Perfetti, P. A. Loukakos, M. Lisowski, U. Bovensiepen, H. Berger, S. Biermann, P. S. Cornaglia, A. Georges, and M. Wolf. Time Evolution of the Electronic Structure of 1T-TaS₂ Through the Insulator-Metal Transition. *Physical Review Letters*, 97(6):067402, 2006.
- [29] F. Schmitt, P. S. Kirchmann, U. Bovensiepen, R. G. Moore, L. Rettig, M. Krenz, J. H. Chu, N. Ru, L. Perfetti, D. H. Lu, M. Wolf, I. R. Fisher, and Z. X. Shen. Transient Electronic Structure and Melting of a Charge Density Wave in TbTe₃. *Science*, 321(5896):1649–1652, 2008.
- [30] Timm Rohwer, Stefan Hellmann, Martin Wiesenmayer, Christian Sohrt, Ankatrin Stange, Bartosz Slomski, Adra Carr, Yanwei Liu, Luis Miaja-Avila, Matthias Kallane, Stefan Mathias, Lutz Kipp, Kai Rossnagel, and Michael Bauer. Collapse of Long-Range Charge Order Tracked by Time-Resolved Photoemission at High Momenta. *Nature*, 471(7339):490–493, 2011.
- [31] J. C. Petersen, S. Kaiser, N. Dean, A. Simoncig, H. Y. Liu, A. L. Cavalieri, C. Cacho, I. C. E.

- Turcu, E. Springate, F. Frassetto, L. Poletto, S. S. Dhesi, H. Berger, and A. Cavalleri. Clocking the Melting Transition of Charge and Lattice Order in 1T-TaS₂ with Ultrafast Extreme-Ultraviolet Angle-Resolved Photoemission Spectroscopy. *Physical Review Letters*, 107(17):177402, 2011.
- [32] M. P. Seah and W. A. Dench. Quantitative Electron Spectroscopy of Surfaces: a Standard Data Base for Electron Inelastic Mean Free Paths in Solids. *Surface and Interface Analysis*, 1(1):2–11, 1979.
- [33] X. J. Zhou, B. Wannberg, W. L. Yang, V. Brouet, Z. Sun, J. F. Douglas, D. Dessau, Z. Hussain, and Z. X. Shen. Space Charge Effect and Mirror Charge Effect in Photoemission Spectroscopy. *Journal of Electron Spectroscopy and Related Phenomena*, 142(1):27–38, 2005.
- [34] S. Passlack, S. Mathias, O. Andreyev, D. Mittnacht, M. Aeschlimann, and M. Bauer. Space Charge Effects in Photoemission with a Low Repetition, High Intensity Femtosecond Laser Source. *Journal of Applied Physics*, 100(2):024912, 2006.
- [35] J. Graf, S. Hellmann, C. Jozwiak, C. L. Smallwood, Z. Hussain, R. A. Kaindl, L. Kipp, K. Rossnagel, and A. Lanzara. Vacuum Space Charge Effect in Laser-Based Solid-State Photoemission Spectroscopy. *Journal of Applied Physics*, 107(1):4095, 2010.
- [36] Joseph Orenstein. Ultrafast Spectroscopy of Quantum Materials. *Physics Today*, 65(9):44–50, 2012.
- [37] A. Tamai, W. Meevasana, P. D. C. King, C. W. Nicholson, A. de la Torre, E. Rozbicki, and F. Baumberger. Spin-Orbit Splitting of the Shockley Surface State on Cu(111). *Physical Review B*, 87(7):075113, 2013.
- [38] E. Carpene, E. Mancini, C. Dallera, G. Ghiringhelli, C. Manzoni, G. Cerullo, and S. De Silvestri. A Versatile Apparatus for Time-Resolved Photoemission Spectroscopy via Femtosecond Pump-Probe Experiments. *Review of Scientific Instruments*, 80(5):055101, 2009.
- [39] F. Schmitt, P. S. Kirchmann, U. Bovensiepen, R. G. Moore, J. H. Chu, D. H. Lu, L. Rettig, M. Wolf, I. R. Fisher, and Z. X. Shen. Ultrafast Electron Dynamics in the Charge Density Wave Material TbTe₃. *New Journal of Physics*, 13:063022, 2011.
- [40] J. Faure, J. Mauchain, E. Papalazarou, W. Yan, J. Pinon, M. Marsi, and L. Perfetti. Full Characterization and Optimization of a Femtosecond Ultraviolet Laser Source for Time and Angle-Resolved Photoemission on Solid Surfaces. *Review of Scientific Instruments*, 83(4):117, 2012.

- [41] J. A. Sobota, S. Yang, J. G. Analytis, Y. L. Chen, I. R. Fisher, P. S. Kirchmann, and Z. X. Shen. Ultrafast Optical Excitation of a Persistent Surface-State Population in the Topological Insulator Bi_2Se_3 . *Physical Review Letters*, 108(11):117403, 2012.
- [42] G. Rohde, A. Hendel, A. Stange, K. Hanff, L. P. Oloff, L. X. Yang, K. Rossnagel, and M. Bauer. Time-Resolved ARPES with Sub-15 fs Temporal and Near Fourier-Limited Spectral Resolution. *Review of Scientific Instruments*, 87(10):103102, 2016.
- [43] B. Frietsch, R. Carley, K. Dobrich, C. Gahl, M. Teichmann, O. Schwarzkopf, P. Wernet, and M. Weinelt. A High-Order Harmonic Generation Apparatus for Time- and Angle-Resolved Photoelectron Spectroscopy. *Review of Scientific Instruments*, 84(7):075106, 2013.
- [44] G. L. Dakovski, Y. Li, T. Durakiewicz, and G. Rodriguez. Tunable Ultrafast Extreme Ultraviolet Source for Time- and Angle-Resolved Photoemission Spectroscopy. *Review of Scientific Instruments*, 81(7):173, 2010.
- [45] P. Siffalovic, M. Drescher, M. Spieweck, T. Wiesenhal, Y. C. Lim, R. Weidner, A. Elizarov, and U. Heinzmann. Laser-Based Apparatus for Extended Ultraviolet Femtosecond Time-Resolved Photoemission Spectroscopy. *Review of Scientific Instruments*, 72(1):30, 2001.
- [46] P. S. Kirchmann, L. Rettig, D. Nandi, U. Lipowski, M. Wolf, and U. Bovensiepen. A Time-of-Flight Spectrometer for Angle-Resolved Detection of Low Energy Electrons in Two Dimensions. *Applied Physics a-Materials Science and Processing*, 91(2):211–217, 2008.
- [47] Zhuojin Xie, Shaolong He, Chaoyu Chen, Ya Feng, Hemian Yi, Aiji Liang, Lin Zhao, Daixiang Mou, Junfeng He, Yingying Peng, Xu Liu, Yan Liu, Guodong Liu, Xiaoli Dong, Li Yu, Jun Zhang, Shenjin Zhang, Zhimin Wang, Fengfeng Zhang, Feng Yang, Qinjun Peng, Xiaoyang Wang, Chuangtian Chen, Zuyan Xu, and X. J. Zhou. Orbital-Selective Spin Texture and its Manipulation in a Topological Insulator. *Nature Communications*, 5:3382, 2014.
- [48] Chenlu Wang, Yan Zhang, Jianwei Huang, Simin Nie, Guodong Liu, Aiji Liang, Yuxiao Zhang, Bing Shen, Jing Liu, Cheng Hu, Ying Ding, Defa Liu, Yong Hu, Shaolong He, Lin Zhao, Li Yu, Jin Hu, Jiang Wei, Zhiqiang Mao, Youguo Shi, Xiaowen Jia, Fengfeng Zhang, Shenjin Zhang, Feng Yang, Zhimin Wang, Qinjun Peng, Hongming Weng, Xi Dai, Zhong Fang, Zuyan Xu, Chuangtian Chen, and X. J. Zhou. Observation of Fermi Arc and Its Connection with Bulk States in the Candidate Type-II Weyl Semimetal WTe_2 . *Physical Review B*, 94(24):241119, 2016.
- [49] I. M. Vishik, W. S. Lee, F. Schmitt, B. Moritz, T. Sasagawa, S. Uchida, K. Fujita, S. Ishida,

- C. Zhang, T. P. Devereaux, and Z. X. Shen. Doping-Dependent Nodal Fermi Velocity of the High-Temperature Superconductor $\text{Bi}_2\text{Sr}_2\text{CaCu}_2\text{O}_{8+\delta}$ Revealed Using High-Resolution Angle-Resolved Photoemission Spectroscopy. *Physical Review Letters*, 104(20):207002, 2010.
- [50] S. Hellmann, M. Beye, C. Sohrt, T. Rohwer, F. Sorgenfrei, H. Redlin, M. Kallaene, M. Marczyński-Buehlow, F. Hennies, M. Bauer, A. Foehlich, L. Kipp, W. Wurth, and K. Rossnagel. Ultrafast Melting of a Charge-Density Wave in the Mott Insulator 1T-TaS₂. *Physical Review Letters*, 105(18):187401, 2010.
- [51] E. Allaria, R. Appio, L. Badano, W. A. Barletta, S. Bassanese, S. G. Biedron, A. Borga, E. Busetto, D. Castronovo, P. Cinquegrana, S. Cleva, D. Cocco, M. Cornacchia, P. Craievich, I. Cudin, G. D’Auria, M. Dal Forno, M. B. Danailov, R. De Monte, G. De Ninno, P. Delgiusto, A. Demidovich, S. Di Mitri, B. Diviacco, A. Fabris, R. Fabris, W. Fawley, M. Ferianis, E. Ferrari, S. Ferry, L. Froehlich, P. Furlan, G. Gaio, F. Gelmetti, L. Giannessi, M. Giannini, R. Gobessi, R. Ivanov, E. Karantzoulis, M. Lonza, A. Lutman, B. Mahieu, M. Milloch, S. V. Milton, M. Musardo, I. Nikolov, S. Noe, F. Parmigiani, G. Penco, M. Petronio, L. Pivetta, M. Predonzani, F. Rossi, L. Rumiz, A. Salom, C. Scafuri, C. Serpico, P. Sigalotti, S. Spampinati, C. Spezzani, M. Svandrlik, C. Svetina, S. Tazzari, M. Trovo, R. Umer, A. Vascotto, M. Veronese, R. Visintini, M. Zaccaria, D. Zangrando, and M. Zangrando. Highly Coherent and Stable Pulses from the FERMI Seeded Free-Electron Laser in the Extreme Ultraviolet. *Nature Photonics*, 6(10):699–704, 2012.
- [52] Xin Zhang, Lirong Wang, Xiaoyang Wang, Guiling Wang, Yong Zhu, and Chuangtian Chen. High-Power Sixth-Harmonic Generation of an Nd:YAG Laser with $\text{KBe}_2\text{BO}_3\text{F}_2$ Prism-Coupled Devices. *Optics Communications*, 285(2122):4519–4522, 2012.
- [53] Chuangtian Chen, Junhua Lu, T. Togashi, T. Suganuma, T. Sekikawa, S. Watanabe, Zuyan Xu, and Jiyang Wang. Second-Harmonic Generation From a $\text{KBe}_2\text{BO}_3\text{F}_2$ Crystal in the Deep Ultraviolet. *Optics Letters*, 27(8):637–639, 2002.
- [54] Matthias Scholz, Dmitrijs Opalevs, Patrick Leisching, Wilhelm Kaenders, Guiling Wang, Xiaoyang Wang, Rukang Li, and Chuangtian Chen. 1.3-mW Tunable and Narrow-Band Continuous-Wave Light Source at 191 nm. *Optics Express*, 20(17):18659–18664, 2012.
- [55] Matthias Scholz, Dmitrijs Opalevs, Patrick Leisching, Wilhelm Kaenders, Guiling Wang, Xiaoyang Wang, Rukang Li, and Chuangtian Chen. A Bright Continuous-Wave Laser Source at 193 nm. *Applied Physics Letters*, 103(5):051114, 2013.

- [56] K. Ishizaka, T. Kiss, T. Yamamoto, Y. Ishida, T. Saitoh, M. Matsunami, R. Eguchi, T. Ohtsuki, A. Kosuge, T. Kanai, M. Nohara, H. Takagi, S. Watanabe, and S. Shin. Femtosecond Core-Level Photoemission Spectroscopy on 1T-TaS₂ Using a 60-eV Laser Source. *Physical Review B*, 83(8):081104, 2011.
- [57] P. B. Corkum. Plasma Perspective on Strong Field Multiphoton Ionization. *Physical Review Letters*, 71(13):1994–1997, 1993.
- [58] M. Bauer. Femtosecond Ultraviolet Photoelectron Spectroscopy of Ultra-Fast Surface Processes. *Journal of Physics D-Applied Physics*, 38(16):R253–R267, 2005.
- [59] S. Hellmann, C. Sohrt, M. Beye, T. Rohwer, F. Sorgenfrei, M. Marczyński-Buehlow, M. Kallaene, H. Redlin, F. Hennies, M. Bauer, A. Foehlich, L. Kipp, W. Wurth, and K. Rossnagel. Time-Resolved X-Ray Photoelectron Spectroscopy at FLASH. *New Journal of Physics*, 14:013062, 2012.
- [60] E. A. Seddon, J. A. Clarke, D. J. Dunning, C. Masciovecchio, C. J. Milne, F. Parmigiani, D. Rugg, J. C. H. Spence, N. R. Thompson, K. Ueda, S. M. Vinko, J. S. Wark, and W. Wurth. Short-Wavelength Free-Electron Laser Sources and Science: A Review. *Reports on Progress in Physics*, 80(11):115901, 2017.
- [61] <https://flash.desy.de/>.
- [62] E. Allaria, A. Battistoni, F. Bencivenga, R. Borghes, C. Callegari, F. Capotondi, D. Castonovo, P. Cinquegrana, D. Cocco, M. Coreno, P. Craievich, R. Cucini, F. D’Amico, M. B. Danailov, A. Demidovich, G. De Ninno, A. Di Cicco, S. Di Fonzo, M. Di Fraia, S. Di Mitri, B. Diviacco, W. M. Fawley, E. Ferrari, A. Filipponi, L. Froehlich, A. Gessini, E. Giangrisostomi, L. Giannessi, D. Giuressi, C. Grazioli, R. Gunnella, R. Ivanov, B. Mahieu, N. Mahne, C. Masciovecchio, I. P. Nikolov, G. Passos, E. Pedersoli, G. Penco, E. Principi, L. Raimondi, R. Sergo, P. Sigalotti, C. Spezzani, C. Svetina, M. Trovo, and M. Zangrando. Tunability Experiments at the FERMI at Elettra Free-electron Laser. *New Journal of Physics*, 14:113009, 2012.
- [63] <https://lcls.slac.stanford.edu/>.
- [64] <http://xfel.riken.jp/eng/index.html>.
- [65] <http://www.xfel.eu/>.
- [66] <https://www.psi.ch/swissfel/>.
- [67] <http://pal.postech.ac.kr/paleng/>.

- [68] D. Wang. Soft X-ray Free Electron Laser at SINAP. *Proceedings of the 7th International Particle Accelerator Conference*, <http://ir.ihep.ac.cn/handle/311005/247348>.
- [69] VUV5000 UV Source(<http://www.scientaomicron.com>).
- [70] UVLS (<http://www.specs.de>).
- [71] S. Souma, T. Sato, T. Takahashi, and P. Baltzer. High-Intensity Xenon Plasma Discharge Lamp for Bulk-Sensitive High-Resolution Photoemission Spectroscopy. *Review of Scientific Instruments*, 78(12):123104, 2007.
- [72] Scienta Analyzer (<http://www.scientaomicron.com>).
- [73] Specs Analyzer (<http://www.specs.de>).
- [74] MB Scientifc 2D Analyzer (<http://www.mbscientific.se>).
- [75] M. H. Berntsen, O. Gotberg, and O. Tjernberg. An Experimental Setup for High Resolution 10.5 eV Laser-Based Angle-Resolved Photoelectron Spectroscopy Using a Time-of-Flight Electron Analyzer. *Review of Scientific Instruments*, 82(9):095113, 2011.
- [76] Y. He, I. M. Vishik, M. Yi, S. Yang, Z. Liu, J. J. Lee, S. Chen, S. N. Rebec, D. Leuenberger, A. Zong, C. M. Jefferson, R. G. Moore, P. S. Kirchmann, A. J. Merriam, and Z. X. Shen. Invited Article: High Resolution Angle Resolved Photoemission with Tabletop 11 eV Laser. *Rev Sci Instrum*, 87(1):011301, 2016.
- [77] C. L. Smallwood, J. P. Hinton, C. Jozwiak, W. T. Zhang, J. D. Koralek, H. Eisaki, D. H. Lee, J. Orenstein, and A. Lanzara. Tracking Cooper Pairs in a Cuprate Superconductor by Ultrafast Angle-Resolved Photoemission. *Science*, 336(6085):1137–1139, 2012.
- [78] C. T. Chen, Z. Y. Xu, D. Q. Deng, J. Zhang, G. K. L. Wong, B. C. Wu, N. Ye, and D. Y. Tang. The Vacuum Ultraviolet Phase-Matching Characteristics of Nonlinear Optical $\text{KBe}_2\text{BO}_3\text{F}_2$ Crystal. *Applied Physics Letters*, 68(21):2930–2932, 1996.
- [79] Tadashi Togashi, Teruto Kanai, Taro Sekikawa, Shuntaro Watanabe, Chuangtian Chen, Chengqian Zhang, Zuyan Xu, and Jiyang Wang. Generation of Vacuum-Ultraviolet Light by An Optically Contacted, Prism-Coupled $\text{KBe}_2\text{BO}_3\text{F}_2$ Crystal. *Optics Letters*, 28(4):254–256, 2003.
- [80] C. T. Chen, G. L. Wang, X. Y. Wang, and Z. Y. Xu. Deep-UV Nonlinear Optical Crystal $\text{KBe}_2\text{BO}_3\text{F}_2$ -Discovery, Growth, Optical Properties and Applications. *Applied Physics B-Lasers and Optics*, 97(1):9–25, 2009.
- [81] Lars Hedin, John Michiels, and John Inglesfield. Transition from the Adiabatic to the Sudden

- Limit in Core-Level Photoemission. *Physical Review B*, 58(23):15565–15582, 1998.
- [82] L. Hedin and J. D. Lee. Sudden Approximation in Photoemission and Beyond. *Journal of Electron Spectroscopy and Related Phenomena*, 124(2):289–315, 2002.
- [83] J. D. Lee, O. Gunnarsson, and L. Hedin. Transition from the Adiabatic to the Sudden Limit in Core-Level Photoemission: A Model Study of A Localized System. *Physical Review B*, 60(11):8034–8049, 1999.
- [84] Mohit Randeria, Hong Ding, J. C. Campuzano, A. Bellman, G. Jennings, T. Yokoya, T. Takahashi, H. Katayama-Yoshida, T. Mochiku, and K. Kadowaki. Momentum Distribution Sum Rule for Angle-Resolved Photoemission. *Physical Review Letters*, 74(24):4951–4954, 1995.
- [85] Shen-jin Zhang, Da-fu Cui, Feng-feng Zhang, Zhi Xu, and Zhi-min and others Wang. High Power All Solid State VUV lasers. *Journal of Electron Spectroscopy and Related Phenomena*, 196:20–23, 2014.
- [86] Yan Zhang, Chenlu Wang, Li Yu, Guodong Liu, Aiji Liang, Jianwei Huang, Simin Nie, Xuan Sun, Yuxiao Zhang, Bing Shen, Jing Liu, Hongming Weng, Lingxiao Zhao, Genfu Chen, Xiaowen Jia, Cheng Hu, Ying Ding, Wenjuan Zhao, Qiang Gao, Cong Li, Shaolong He, Lin Zhao, Fengfeng Zhang, Shenjin Zhang, Feng Yang, Zhimin Wang, Qinjun Peng, Xi Dai, Zhong Fang, Zuyan Xu, Chuangtian Chen, and X. J. Zhou. Electronic evidence of temperature-induced Lifshitz transition and topological nature in ZrTe₅. *Nature Communications*, 8:15512, 2017.
- [87] Rui Jiang, Daixiang Mou, Yun Wu, Lunan Huang, Colin D. McMillen, Joseph Kolis, III Giesber, Henry G., John J. Egan, and Adam Kaminski. Tunable Vacuum Ultraviolet Laser Based Spectrometer for Angle Resolved Photoemission Spectroscopy. *Review of Scientific Instruments*, 85(3):033902, 2014.
- [88] Lunan Huang, Timothy M. McCormick, Masayuki Ochi, Zhiying Zhao, Michi-To Suzuki, Ryotaro Arita, Yun Wu, Daixiang Mou, Huibo Cao, Jiaqiang Yan, Nandini Trivedi, and Adam Kaminski. Spectroscopic Evidence for a Type II Weyl Semimetallic State in MoTe₂. *Nat Mater*, 15(11):1155–1160, 2016.
- [89] Yun Wu, Daixiang Mou, Na Hyun Jo, Kewei Sun, Lunan Huang, S. L. Bud’ko, P. C. Canfield, and Adam Kaminski. Observation of Fermi Arcs in the Type-II Weyl Semimetal Candidate WTe₂. *Physical Review B*, 94(12):121113, 2016.
- [90] M. Z. Hasan and C. L. Kane. Colloquium: Topological Insulators. *Reviews of Modern*

- Physics*, 82(4):3045–3067, 2010.
- [91] Xiao-Liang Qi and Shou-Cheng Zhang. Topological Insulators and Superconductors. *Reviews of Modern Physics*, 83(4):1057–1110, 2011.
 - [92] S. A. Wolf, D. D. Awschalom, R. A. Buhrman, J. M. Daughton, S. von Molnar, M. L. Roukes, A. Y. Chtchelkanova, and D. M. Treger. Spintronics: A Spin-based Electronics Vision for the Future. *Science*, 294(5546):1488–1495, 2001.
 - [93] N. F. Mott. The Scattering of Fast Electrons by Atomic Nuclei. *Proceedings of the Royal Society of London Series a-Containing Papers of a Mathematical and Physical Character*, 124(794):425–442, 1929.
 - [94] N. F. Mott. The Polarisation of Electrons by Double Scattering. *Proceedings of the Royal Society of London Series a-Containing Papers of a Mathematical and Physical Character*, 135(827):429–458, 1932.
 - [95] J. Kirschner and R. Feder. Spin Polarization in Double Diffraction of Low-Energy Electrons from W(001) - Experiment and Theory. *Physical Review Letters*, 42(15):1008–1011, 1979.
 - [96] J. Unguris, D. T. Pierce, and R. J. Celotta. Low-Energy Diffuse-Scattering Electron-Spin Polarization Analyzer. *Review of Scientific Instruments*, 57(7):1314–1323, 1986.
 - [97] D. Tillmann, R. Thiel, and E. Kisker. Very-Low-Energy Spin-Polarized Electron-Diffraction from Fe(001). *Zeitschrift Fur Physik B-Condensed Matter*, 77(1):1–2, 1989.
 - [98] R. Bertacco, M. Merano, and F. Ciccacci. Spin Dependent Electron Absorption in Fe(001)-p(1x1)O: a New Candidate for a Stable and Efficient Electron Polarization Analyzer. *Applied Physics Letters*, 72(16):2050–2052, 1998.
 - [99] T. Okuda, Y. Takeichi, A. Harasawa, I. Matsuda, T. Kinoshita, and A. Kakizaki. High Efficiency and High Energy-Resolution Spin-Polarized Photoemission Spectrometer. *European Physical Journal-Special Topics*, 169:181–185, 2009.
 - [100] F. U. Hillebrecht, R. M. Jungblut, L. Wiebusch, C. Roth, H. B. Rose, D. Knabben, C. Bethke, N. B. Weber, S. Manderla, U. Rosowski, and E. Kisker. High-Efficiency Spin Polarimetry by Very-Low-Energy Electron Scattering from Fe(100) for Spin-Resolved Photoemission. *Review of Scientific Instruments*, 73(3):1229–1234, 2002.
 - [101] S. Qiao, A. Kimura, A. Harasawa, M. Sawada, J. G. Chung, and A. Kakizaki. A New Compact Electron Spin Polarimeter with a High Efficiency. *Review of Scientific Instruments*, 68(12):4390–4395, 1997.

- [102] M. Hoesch, T. Greber, V. Petrov, A. Muntwiler, M. Hengsberger, W. Auwärter, and J. Osterwalder. Spin-Polarized Fermi Surface Mapping. *Journal of Electron Spectroscopy and Related Phenomena*, 124(2-3):263–279, 2002.
- [103] D. D. Neufeld, H. Aliabadi, and F. B. Dunning. Compact Retarding-Potential Mott Polarimeter. *Review of Scientific Instruments*, 78(2):025107, 2007.
- [104] S. Souma, A. Takayama, K. Sugawara, T. Sato, and T. Takahashi. Ultrahigh-Resolution Spin-Resolved Photoemission Spectrometer with a Mini Mott Detector. *Review of Scientific Instruments*, 81(9):095101, 2010.
- [105] Christian Tusche, Alexander Krasnyuk, and Jürgen Kirschner. Spin Resolved Bandstructure Imaging with a High Resolution Momentum Microscope. *Ultramicroscopy*, 159:520(10), 2015.
- [106] Koichiro Yaji, Ayumi Harasawa, Kenta Kuroda, Sogen Toyohisa, Mitsuhiro Nakayama, Yukiaki Ishida, Akiko Fukushima, Shuntaro Watanabe, Chuangtian Chen, Fumio Komori, and Shik Shin. High-Resolution Three-Dimensional Spin- and Angle-Resolved Photoelectron Spectrometer Using Vacuum Ultraviolet Laser Light. *Review of Scientific Instruments*, 87(5):053111, 2016.
- [107] E. I. Rashba. Properties of Semiconductors with An Extremum Loop.1.Cyclotron and Combinational Resonance in a Magnetic Field Perpendicular to the Plane of the Loop. *Soviet Physics-Solid State*, 2(6):1109–1122, 1960.
- [108] Y. A. Bychkov and E. I. Rashba. Properties of a 2D Electron-Gas with Lifted Spectral Degeneracy. *Jetp Letters*, 39(2):78–81, 1984.
- [109] S. LaShell, B. A. McDougall, and E. Jensen. Spin Splitting of an Au(111) Surface State Band Observed with Angle Resolved Photoelectron Spectroscopy. *Physical Review Letters*, 77(16):3419–3422, 1996.
- [110] G. Nicolay, F. Reinert, S. Hüfner, and P. Blaha. Spin-Orbit Splitting of the L -Gap Surface State on Au(111) and Ag(111). *Physical Review B*, 65(3):033407, 2001.
- [111] J. Henk, M. Hoesch, J. Osterwalder, A. Ernst, and P. Bruno. Spin-Orbit Coupling in the L-Gap Surface States of Au(111): Spin-Resolved Photoemission Experiments and First-Principles Calculations. *Journal of Physics-Condensed Matter*, 16(43):7581–7597, 2004.
- [112] J. Hugo Dil. Spin and Angle Resolved Photoemission on Non-Magnetic Low-Dimensional Systems. *Journal of Physics-Condensed Matter*, 21(40):403001, 2009.
- [113] T. Valla, A. V. Fedorov, P. D. Johnson, B. O. Wells, S. L. Hulbert, Q. Li, G. D. Gu, and

- N. Koshizuka. Evidence for Quantum Critical Behavior in the Optimally Doped Cuprate $\text{Bi}_2\text{Sr}_2\text{CaCu}_2\text{O}_{8+\delta}$. *Science*, 285(5436):2110–2113, 1999.
- [114] Y. H. Wang, D. Hsieh, E. J. Sie, H. Steinberg, D. R. Gardner, Y. S. Lee, P. Jarillo-Herrero, and N. Gedik. Measurement of Intrinsic Dirac Fermion Cooling on the Surface of the Topological Insulator Bi_2Se_3 Using Time-Resolved and Angle-Resolved Photoemission Spectroscopy. *Physical Review Letters*, 109(12):127401, 2012.
- [115] www.lumeras-labs.com.
- [116] T. J. Reber, N. C. Plumb, J. A. Waugh, and D. S. Dessau. Effects, Determination, and Correction of Count Rate Nonlinearity in Multi-Channel Analog Electron Detectors. *Review of Scientific Instruments*, 85(4):017005, 2014.
- [117] K. Nasu, H. Ping, and H. Mizouchi. Photoinduced Structural Phase Transitions and Their Dynamics. *Journal of Physics-Condensed Matter*, 13(35):R693–R721, 2001.
- [118] N. Takubo, Y. Ogimoto, M. Nakamura, H. Tamaru, M. Izumi, and K. Miyano. Persistent and Reversible All-Optical Phase Control in a Manganite Thin Film. *Physical Review Letters*, 95(1):017404, 2005.
- [119] D. Polli, M. Rini, S. Wall, R. W. Schoenlein, Y. Tomioka, Y. Tokura, G. Cerullo, and A. Cavalleri. Coherent Orbital Waves in the Photo-Induced Insulator-Metal Dynamics of a Magnetoresistive Manganite. *Nature Materials*, 6(9):643–647, 2007.
- [120] Mengkun Liu, Harold Y. Hwang, Hu Tao, Andrew C. Strikwerda, Kebin Fan, George R. Keiser, Aaron J. Sternbach, Kevin G. West, Salinporn Kittiwatanakul, Jiwei Lu, Stuart A. Wolf, Fiorenzo G. Omenetto, Xin Zhang, Keith A. Nelson, and Richard D. Averitt. Terahertz-Field-Induced Insulator-to-Metal Transition in Vanadium Dioxide Metamaterial. *Nature*, 487(7407):345–348, 2012.
- [121] Vance R. Morrison, Robert P. Chatelain, Kunal L. Tiwari, Ali Hendaoui, Andrew Bruhacs, Mohamed Chaker, and Bradley J. Siwick. A Photoinduced Metal-Like Phase of Monoclinic VO_2 Revealed by Ultrafast Electron Diffraction. *Science*, 346(6208):445–448, 2014.
- [122] Jingdi Zhang, Xuelian Tan, Mengkun Liu, S. W. Teitelbaum, K. W. Post, Feng Jin, K. A. Nelson, D. N. Basov, Wenbin Wu, and R. D. Averitt. Cooperative Photoinduced Metastable Phase Control in Strained Manganite Films. *Nature Materials*, 15(9):956–960, 2016.
- [123] Sven A. Donges, Omar Khatib, Brian T. O’Callahan, Joanna M. Atkin, Jae Hyung Park, David Cobden, and Markus B. Raschke. Ultrafast Nanoimaging of the Photoinduced Phase

- Transition Dynamics in VO₂. *Nano Letters*, 16(5):3029–3035, 2016.
- [124] K. W. Kim, A. Pashkin, H. Schaefer, M. Beyer, M. Porer, T. Wolf, C. Bernhard, J. Demsar, R. Huber, and A. Leitenstorfer. Ultrafast Transient Generation of Spin-Density-Wave Order in the Normal State of BaFe₂As₂ Driven by Coherent Lattice Vibrations. *Nature Materials*, 11(6):497–501, 2012.
 - [125] L. Stojchevska, I. Vaskivskiy, T. Mertelj, P. Kusar, D. Svetin, S. Brazovskii, and D. Mihailovic. Ultrafast Switching to a Stable Hidden Quantum State in an Electronic Crystal. *Science*, 344(6180):177–180, 2014.
 - [126] A. Singer, S. K. K. Patel, R. Kukreja, V. Uhler, J. Wingert, S. Festersen, D. Zhu, J. M. Glowia, H. T. Lemke, S. Nelson, M. Kozina, K. Rossnagel, M. Bauer, B. M. Murphy, O. M. Magnussen, E. E. Fullerton, and O. G. Shpyrko. Photoinduced Enhancement of the Charge Density Wave Amplitude. *Physical Review Letters*, 117(5):056401, 2016.
 - [127] D. Fausti, R. I. Tobey, N. Dean, S. Kaiser, A. Dienst, M. C. Hoffmann, S. Pyon, T. Takayama, H. Takagi, and A. Cavalleri. Light-Induced Superconductivity in a Stripe-Ordered Cuprate. *Science*, 331(6014):189–191, 2011.
 - [128] W. Hu, S. Kaiser, D. Nicoletti, C. R. Hunt, I. Gierz, M. C. Hoffmann, M. Le Tacon, T. Loew, B. Keimer, and A. Cavalleri. Optically Enhanced Coherent Transport in YBa₂Cu₃O_{6.5} by Ultrafast Redistribution of Interlayer Coupling. *Nature Materials*, 13(7):705–711, 2014.
 - [129] M. Mitrano, A. Cantaluppi, D. Nicoletti, S. Kaiser, A. Perucchi, S. Lupi, P. Di Pietro, D. Pontiroli, M. Ricco, S. R. Clark, D. Jaksch, and A. Cavalleri. Possible Light-Induced Superconductivity in K₃C₆₀ at High Temperature. *Nature*, 530(7591):461, 2016.
 - [130] S. P. Weathersby, G. Brown, M. Centurion, T. F. Chase, R. Coffee, J. Corbett, J. P. Eichner, J. C. Frisch, A. R. Fry, M. Guehr, N. Hartmann, C. Hast, R. Hettel, R. K. Jobe, E. N. Jongewaard, J. R. Lewandowski, R. K. Li, A. M. Lindenberg, I. Makasyuk, J. E. May, D. McCormick, M. N. Nguyen, A. H. Reid, X. Shen, K. Sokolowski-Tinten, T. Vecchione, S. L. Vetter, J. Wu, J. Yang, H. A. Duerr, and X. J. Wang. Mega-electron-volt ultrafast electron diffraction at SLAC National Accelerator Laboratory. *Review of Scientific Instruments*, 86(7):073702, 2015.
 - [131] G. Hartmann, A. O. Lindahl, A. Knie, N. Hartmann, A. A. Lutman, J. P. MacArthur, I. Shevchuk, J. Buck, A. Galler, J. M. Glowia, W. Helml, Z. Huang, N. M. Kabachnik, A. K. Kazansky, J. Liu, A. Marinelli, T. Mazza, H. D. Nuhn, P. Walter, J. Viehhaus, M. Meyer,

- S. Moeller, R. N. Coffee, and M. Ilchen. Circular Dichroism Measurements at An X-Ray Free-Electron Laser with Polarization Control. *Review of Scientific Instruments*, 87(8):641, 2016.
- [132] L. Perfetti, P. A. Loukakos, M. Lisowski, U. Bovensiepen, H. Eisaki, and M. Wolf. Ultrafast Electron Relaxation in Superconducting $\text{Bi}_2\text{Sr}_2\text{CaCu}_2\text{O}_{8+\delta}$ by Time-Resolved Photoelectron Spectroscopy. *Physical Review Letters*, 99(19):197001, 2007.
- [133] C. L. Smallwood, C. Jozwiak, W. T. Zhang, and A. Lanzara. An Ultrafast Angle-Resolved Photoemission Apparatus for Measuring Complex Materials. *Review of Scientific Instruments*, 83(12):123904–123904–6, 2012.
- [134] K. Kummer, D. V. Vyalikh, L. Rettig, R. Cortes, Yu Kucherenko, C. Krellner, C. Geibel, U. Bovensiepen, M. Wolf, and S. L. Molodtsov. Ultrafast Quasiparticle Dynamics in the Heavy-Fermion Compound YbRh_2Si_2 . *Physical Review B*, 86(8):4583–4586, 2012.
- [135] L. Rettig, R. Cortes, S. Thirupathaiah, P. Gegenwart, H. S. Jeevan, M. Wolf, J. Fink, and U. Bovensiepen. Ultrafast Momentum-Dependent Response of Electrons in Antiferromagnetic EuFe_2As_2 Driven by Optical Excitation. *Physical Review Letters*, 108(9):097002, 2012.
- [136] L. X. Yang, G. Rohde, T. Rohwer, A. Stange, K. Hanff, C. Sohrt, L. Rettig, R. Cortes, F. Chen, D. L. Feng, T. Wolf, B. Kamble, I. Eremin, T. Popmintchev, M. M. Murnane, H. C. Kapteyn, L. Kipp, J. Fink, M. Bauer, U. Bovensiepen, and K. Rossnagel. Ultrafast Modulation of the Chemical Potential in BaFe_2As_2 by Coherent Phonons. *Physical Review Letters*, 112(20):207001, 2014.
- [137] Wentao Zhang, Choongyu Hwang, Christopher L. Smallwood, Tristan L. Miller, Gregory Affeldt, Koshi Kurashima, Chris Jozwiak, Hiroshi Eisaki, Tadashi Adachi, Yoji Koike, Dung-Hai Lee, and Alessandra Lanzara. Ultrafast Quenching of Electron-Boson Interaction and Superconducting Gap in a Cuprate Superconductor. *Nature Communications*, 5:4959, 2014.
- [138] J. D. Rameau, S. Freutel, L. Rettig, I. Avigo, M. Ligges, Y. Yoshida, H. Eisaki, J. Schneeloch, R. D. Zhong, Z. J. Xu, G. D. Gu, P. D. Johnson, and U. Bovensiepen. Photoinduced Changes in the Cuprate Electronic Structure Revealed by Femtosecond Time- and Angle-Resolved Photoemission. *Physical Review B*, 89(11):867–875, 2014.
- [139] S. L. Yang, J. A. Sobota, D. Leuenberger, Y. He, M. Hashimoto, D. H. Lu, H. Eisaki, P. S. Kirchmann, and Z. X. Shen. Inequivalence of Single-Particle and Population Lifetimes in a Cuprate Superconductor. *Physical Review Letters*, 114(24):247001, 2015.

- [140] M. Hajlaoui, E. Papalazarou, J. Mauchain, Z. Jiang, I. Miotkowski, Y. P. Chen, A. Taleb-Ibrahimi, L. Perfetti, and M. Marsi. Time Resolved Ultrafast ARPES for the Study of Topological Insulators: The Case of Bi_2Te_3 . *European Physical Journal-Special Topics*, 222(5):1271–1275, 2013.
- [141] A. Crepaldi, F. Cilento, B. Ressel, C. Cacho, J. C. Johannsen, M. Zacchigna, H. Berger, Ph Bugnon, C. Grazioli, I. C. E. Turcu, E. Springate, K. Kern, M. Grioni, and F. Parmigiani. Evidence of Reduced Surface Electron-Phonon Scattering in the Conduction Band of Bi_2Se_3 by Nonequilibrium ARPES. *Physical Review B*, 88(12):95–103, 2013.
- [142] J. A. Sobota, S. L. Yang, D. Leuenberger, A. F. Kemper, J. G. Analytis, I. R. Fisher, P. S. Kirchmann, T. P. Devereaux, and Z. X. Shen. Distinguishing Bulk and Surface Electron-Phonon Coupling in the Topological Insulator Bi_2Se_3 Using Time-Resolved Photoemission Spectroscopy. *Physical Review Letters*, 113(15):157401, 2014.
- [143] H. Y. Liu, I. Gierz, J. C. Petersen, S. Kaiser, A. Simoncig, A. L. Cavalieri, C. Cacho, I. C. E. Turcu, E. Springate, F. Frassetto, L. Poletto, S. S. Dhesi, Z. A. Xu, T. Cuk, R. Merlin, and A. Cavalleri. Possible Observation of Parametrically Amplified Coherent Phonons in $\text{K}_{0.3}\text{MoO}_3$ Using Time-Resolved Extreme-Ultraviolet Angle-Resolved Photoemission Spectroscopy. *Physical Review B*, 88(4):3239–3246, 2013.
- [144] A. L. Cavalieri, N. Mueller, Th Uphues, V. S. Yakovlev, A. Baltuska, B. Horvath, B. Schmidt, L. Bluemel, R. Holzwarth, S. Hendel, M. Drescher, U. Kleineberg, P. M. Echenique, R. Kienberger, F. Krausz, and U. Heinzmann. Attosecond Spectroscopy in Condensed Matter. *Nature*, 449(7165):1029–1032, 2007.
- [145] E. Papalazarou, J. Faure, J. Mauchain, M. Marsi, A. Taleb-Ibrahimi, I. Reshetnyak, A. van Roekeghem, I. Timrov, N. Vast, B. Arnaud, and L. Perfetti. Coherent Phonon Coupling to Individual Bloch States in Photoexcited Bismuth. *Physical Review Letters*, 108(25):456–463, 2012.
- [146] S. Ulstrup, J. C. Johannsen, A. Crepaldi, F. Cilento, M. Zacchigna, C. Cacho, R. T. Chapman, E. Springate, F. Fromm, C. Roidel, T. Seyller, F. Parmigiani, M. Grioni, and P. Hofmann. Ultrafast Electron Dynamics in Epitaxial Graphene Investigated with Time- and Angle-Resolved Photoemission Spectroscopy. *Journal of Physics-Condensed Matter*, 27(16):164206, 2015.
- [147] Zhensheng Tao, Cong Chen, Tibor Szilvasi, Mark Keller, Manos Mavrikakis, Henry Kapteyn,

- and Margaret Murnane. Direct Time-Domain Observation of Attosecond Final-State Lifetimes in Photoemission from Solids. *Science*, 353(6294):62–67, 2016.
- [148] A. Sterzi, A. Crepaldi, F. Cilento, G. Manzoni, E. Frantzeskakis, M. Zacchigna, E. van Heumen, Y. K. Huang, M. S. Golden, and F. Parmigiani. SmB₆ Electron-Phonon Coupling Constant from Time- and Angle-Resolved Photoelectron Spectroscopy. *Physical Review B*, 94(8):081111, 2016.
- [149] Y. Ishida, T. Togashi, K. Yamamoto, M. Tanaka, T. Kiss, T. Otsu, Y. Kobayashi, and S. Shin. Time-Resolved Photoemission Apparatus Achieving Sub-20-meV Energy Resolution and High Stability. *Rev Sci Instrum*, 85(12):123904, 2014.
- [150] L. Nugent-Glandorf, M. Scheer, D. A. Samuels, V. Bierbaum, and S. R. Leone. A laser-Based Instrument for the Study of Ultrafast Chemical Dynamics by Soft X-Ray-Probe Photoelectron Spectroscopy. *Review of Scientific Instruments*, 73(4):1875–1886, 2002.
- [151] Philippe Wernet, Jerome Gaudin, Kai Godehusen, Olaf Schwarzkopf, and Wolfgang Eberhardt. Femtosecond Time-Resolved Photoelectron Spectroscopy with a Vacuum-Ultraviolet Photon Source Based on Laser High-order Harmonic Generation. *Review of Scientific Instruments*, 82(6):443–R, 2011.
- [152] He Wang, Yiming Xu, Stefan Ulonska, Joseph S. Robinson, Predrag Ranitovic, and Robert A. Kaindl. Bright High-Repetition-Rate Source of Narrowband Extreme-Ultraviolet Harmonics Beyond 22 eV. *Nature Communications*, 6:7459, 2015.
- [153] A. von Conta, M. Huppert, and H. J. Worner. A Table-Top Monochromator for Tunable Femtosecond XUV Pulses Generated in a Semi-Infinite Gas Cell: Experiment and Simulations. *Review of Scientific Instruments*, 87(7):073102, 2016.
- [154] F. Cilento, A. Crepaldi, G. Manzoni, A. Sterzi, M. Zacchigna, P. Bugnon, H. Berger, and F. Parmigiani. Advancing Non-Equilibrium ARPES Experiments by a 9.3 eV Coherent Ultrafast Photon Source. *Journal of Electron Spectroscopy and Related Phenomena*, 207:7–13, 2016.
- [155] A. Pietzsch, A. Foehlich, M. Beye, M. Deppe, F. Hennies, M. Nagasono, E. Suljoti, W. Wurth, C. Gahl, K. Doebrich, and A. Melnikov. Towards Time Resolved Core Level Photoelectron Spectroscopy with Femtosecond X-ray Free-Electron Lasers. *New Journal of Physics*, 10:033004, 2008.
- [156] L. P. Oloff, M. Oura, K. Rossnagel, A. Chainani, M. Matsunami, R. Eguchi, T. Kiss,

- Y. Nakatani, T. Yamaguchi, J. Miyawaki, M. Taguchi, K. Yamagami, T. Togashi, T. Katayama, K. Ogawa, M. Yabashi, and T. Ishikawa. Time-Resolved HAXPES at SACLA: Probe and Pump Pulse-Induced Space-Charge Effects. *New Journal of Physics*, 16:123045, 2014.
- [157] P. V. Bogdanov, A. Lanzara, S. A. Kellar, X. J. Zhou, E. D. Lu, W. J. Zheng, G. Gu, J. I. Shimoyama, K. Kishio, H. Ikeda, R. Yoshizaki, Z. Hussain, and Z. X. Shen. Evidence for an Energy Scale for Quasiparticle Dispersion in $\text{Ba}_2\text{Sr}_2\text{CaCu}_2\text{O}_{8+\delta}$. *Physical Review Letters*, 85(12):2581–2584, 2000.
- [158] A. Kaminski, M. Randeria, J. C. Campuzano, M. R. Norman, H. Fretwell, J. Mesot, T. Sato, T. Takahashi, and K. Kadowaki. Renormalization of Spectral Line Shape and Dispersion below T_c in $\text{Ba}_2\text{Sr}_2\text{CaCu}_2\text{O}_{8+\delta}$. *Physical Review Letters*, 86(6):1070–1073, 2001.
- [159] P. D. Johnson, T. Valla, A. V. Fedorov, Z. Yusof, B. O. Wells, Q. Li, A. R. Moodenbaugh, G. D. Gu, N. Koshizuka, C. Kendziora, Sha Jian, and D. G. Hinks. Doping and Temperature Dependence of the Mass Enhancement Observed in the Cuprate $\text{Ba}_2\text{Sr}_2\text{CaCu}_2\text{O}_{8+\delta}$. *Physical Review Letters*, 87(17):177007, 2001.
- [160] A. Lanzara, P. V. Bogdanov, X. J. Zhou, S. A. Kellar, D. L. Feng, E. D. Lu, T. Yoshida, H. Eisaki, A. Fujimori, K. Kishio, J. I. Shimoyama, T. Noda, S. Uchida, Z. Hussain, and Z. X. Shen. Evidence for ubiquitous strong electron-phonon coupling in high-temperature superconductors. *Nature*, 412(6846):510–514, 2001.
- [161] X. J. Zhou, T. Yoshida, A. Lanzara, P. V. Bogdanov, S. A. Kellar, K. M. Shen, W. L. Yang, F. Ronning, T. Sasagawa, T. Kakeshita, T. Noda, H. Eisaki, S. Uchida, C. T. Lin, F. Zhou, J. W. Xiong, W. X. Ti, Z. X. Zhao, A. Fujimori, Z. Hussain, and Z. X. Shen. High-Temperature Superconductors: Universal Nodal Fermi Velocity. *Nature*, 423(6938):398–398, 2003.
- [162] Junren Shi, S. J. Tang, Biao Wu, P. T. Sprunger, W. L. Yang, V. Brouet, X. J. Zhou, Z. Hussain, Z. X. Shen, Zhenyu Zhang, and E. W. Plummer. Direct Extraction of the Eliashberg Function for Electron-Phonon Coupling: a Case Study of $\text{Be}(10\bar{1}0)$. *Physical Review Letters*, 92(18):186401, 2004.
- [163] Wentao Zhang, Guodong Liu, Jianqiao Meng, Lin Zhao, Haiyun Liu, Xiaoli Dong, Wei Lu, J. S. Wen, Z. J. Xu, G. D. Gu, T. Sasagawa, Guiling Wang, Yong Zhu, Hongbo Zhang, Yong Zhou, Xiaoyang Wang, Zhongxian Zhao, Chuangtian Chen, Zuyan Xu, and X. J. Zhou. High

- Energy Dispersion Relations for the High Temperature $\text{Ba}_2\text{Sr}_2\text{CaCu}_2\text{O}_{8+\delta}$ Superconductor from Laser-Based Angle-Resolved Photoemission Spectroscopy. *Physical Review Letters*, 101(1):017002, 2008.
- [164] R. J. McQueeney, J. L. Sarrao, P. G. Pagliuso, P. W. Stephens, and R. Osborn. Mixed Lattice and Electronic States in High-Temperature Superconductors. *Physical Review Letters*, 87(7):077001, 2001.
- [165] Pengcheng Dai, H. A. Mook, S. M. Hayden, G. Aeppli, T. G. Perring, R. D. Hunt, and F. Doan. The Magnetic Excitation Spectrum and Thermodynamics of High-Tc Superconductors. *Science*, 284(5418):1344, 1999.
- [166] H. F. Fong, P. Bourges, Y. Sidis, L. P. Regnault, J. Bossy, A. Ivanov, D. L. Milius, I. A. Aksay, and B. Keimer. Spin Susceptibility in Underdoped $\text{YBa}_2\text{Cu}_3\text{O}_{6+x}$. *Physical Review B*, 61(21):14773–14786, 2000.
- [167] J. Hwang, T. Timusk, E. Schachinger, and J. P. Carbotte. Evolution of the Bosonic Spectral Density of the High-Temperature Superconductor $\text{Bi}_2\text{Sr}_2\text{CaCu}_2\text{O}_{8+\delta}$. *Physical Review B*, 75(14):144508–6, 2007.
- [168] I. Giaever, H. R. Hart, and K. Megerle. Tunneling into Superconductors at Temperatures below 1 K. *Physical Review*, 126(3):941–948, 1962.
- [169] W. L. McMillan and J. M. Rowell. Lead Phonon Spectrum Calculated from Superconducting Density of States. *Physical Review Letters*, 14(4):108–112, 1965.
- [170] I. Vekhter and C. M. Varma. Proposal to Determine the Spectrum of Pairing Glue in High-Temperature Superconductors. *Physical Review Letters*, 90(23):237003, 2003.
- [171] Jin Mo Bok, Jae Hyun Yun, Han-Yong Choi, Wentao Zhang, X. J. Zhou, and Chandra M. Varma. Momentum Dependence of the Single-Particle Self-energy and Fluctuation Spectrum of Slightly Underdoped $\text{Bi}_2\text{Sr}_2\text{CaCu}_2\text{O}_{8+\delta}$ from high-resolution laser angle-resolved photoemission. *Physical Review B*, 81(17):174516, 2010.
- [172] Jin Mo Bok, Jong Ju Bae, Han-Yong Choi, Chandra M. Varma, Wentao Zhang, Junfeng He, Yuxiao Zhang, Li Yu, and X. J. Zhou. Quantitative Determination of Pairing Interactions for High-Temperature Superconductivity in Cuprates. *Science Advances*, 2(3):e1501329, 2016.
- [173] Haijun Zhang, Chao-Xing Liu, and Shou-Cheng Zhang. Spin-Orbital Texture in Topological Insulators. *Physical Review Letters*, 111(6):066801, 2013.
- [174] Mazhar N. Ali, Jun Xiong, Steven Flynn, Jing Tao, Quinn D. Gibson, Leslie M. Schoop,

- Tian Liang, Neel Haldolaarachchige, Max Hirschberger, N. P. Ong, and R. J. Cava. Large, Non-Saturating Magnetoresistance in WTe_2 . *Nature*, 514(7521):205–208, 2014.
- [175] Alexey A. Soluyanov, Dominik Gresch, Zhijun Wang, QuanSheng Wu, Matthias Troyer, Xi Dai, and B. Andrei Bernevig. Type-II Weyl Semimetals. *Nature*, 527(7579):495–498, 2015.
- [176] Chenlu Wang, Yan Zhang, Jianwei Huang, Guodong Liu, Aiji Liang, Yuxiao Zhang, Bing Shen, Jing Liu, Cheng Hu, Ying Ding, Dafa Liu, Yong Hu, Shaolong He, Lin Zhao, Li Yu, Jin Hu, Jiang Wei, Zhiqiang Mao, Youguo Shi, Xiaowen Jia, Fengfeng Zhang, Shenjin Zhang, Feng Yang, Zhimin Wang, Qinqun Peng, Zuyan Xu, Chuangtian Chen, and Xingjiang Zhou. Evidence of Electron Hole Imbalance in WTe_2 from High Resolution Angle Resolved Photoemission Spectroscopy. *Chinese Physics Letters*, 34:097305, 2017.
- [177] Hongming Weng, Xi Dai, and Zhong Fang. Transition-Metal Pentatelluride ZrTe_5 and HfTe_5 : A Paradigm for Large-Gap Quantum Spin Hall Insulators. *Physical Review X*, 4(1):011002, 2014.
- [178] R. Cortes, L. Rettig, Y. Yoshida, H. Eisaki, M. Wolf, and U. Bovensiepen. Momentum-Resolved Ultrafast Electron Dynamics in Superconducting $\text{Bi}_2\text{Sr}_2\text{CaCu}_2\text{O}_{8+\delta}$. *Physical Review Letters*, 107(9):097002, 2011.
- [179] Wentao Zhang, Christopher L. Smallwood, Chris Jozwiak, Tristan L. Miller, Yoshiyuki Yoshida, Hiroshi Eisaki, Dung-Hai Lee, and Alessandra Lanzara. Signatures of Superconductivity and Pseudogap Formation in Nonequilibrium Nodal Quasiparticles Revealed by Ultrafast Angle-Resolved Photoemission. *Physical Review B*, 88(24):245132, 2013.
- [180] Christopher L. Smallwood, Wentao Zhang, Tristan L. Miller, Chris Jozwiak, Hiroshi Eisaki, Dung-Hai Lee, and Alessandra Lanzara. Time- and Momentum-Resolved Gap Dynamics in $\text{Bi}_2\text{Sr}_2\text{CaCu}_2\text{O}_{8+\delta}$. *Physical Review B*, 89(11):115126, 2014.
- [181] Y. H. Wang, H. Steinberg, P. Jarillo-Herrero, and N. Gedik. Observation of Floquet-Bloch States on the Surface of a Topological Insulator. *Science*, 342(6157):453–457, 2013.
- [182] J. A. Sobota, S. L. Yang, A. F. Kemper, J. J. Lee, F. T. Schmitt, W. Li, R. G. Moore, J. G. Analytis, I. R. Fisher, P. S. Kirchmann, T. P. Devereaux, and Z. X. Shen. Direct Optical Coupling to an Unoccupied Dirac Surface State in the Topological Insulator Bi_2Se_3 . *Physical Review Letters*, 111(13):136802, 2013.
- [183] T. Taniuchi, Y. Kotani, and S. Shin. Ultrahigh-Spatial-Resolution Chemical and Magnetic

Imaging by Laser-Based Photoemission Electron Microscopy. *Review of Scientific Instruments*, 86(2):023701, 2015.

[184] <https://www.ifw-dresden.de/institutes/iff/synchrotron-methods/1-cubed-arpes/>.

[185] <http://laser-arpes.cn/en/>.

[186] K. Okazaki, Y. Ota, Y. Kotani, W. Malaeb, Y. Ishida, T. Shimojima, T. Kiss, S. Watanabe, C. T. Chen, K. Kihou, C. H. Lee, A. Iyo, H. Eisaki, T. Saito, H. Fukazawa, Y. Kohori, K. Hashimoto, T. Shibauchi, Y. Matsuda, H. Ikeda, H. Miyahara, R. Arita, A. Chainani, and S. Shin. Octet-Line Node Structure of Superconducting Order Parameter in KFe_2As_2 . *Science*, 337(6100):1314–1317, 2012.

Acknowledgements We acknowledge collaborations with Prof. Zuyan Xu’s group and Prof. Chuangtian Chen’s group in developing laser-based photoemission systems over many years, and Prof. Chandra Varma and Prof. Han-Yong Choi for collaborations in data analysis and discussions. We acknowledge permission of using the FEL sketch provided by Siegfried Schreiber in DESY - FLASH. XJZ thanks the funding support by the National Key Research and Development Program of China (2016YFA0300300), the National Science Foundation of China (11334010), the Strategic Priority Research Program (B) of the Chinese Academy of Sciences (Grant No. XDB07020300), and . Wentao Zhang was sponsored by Shanghai Pujiang Program.

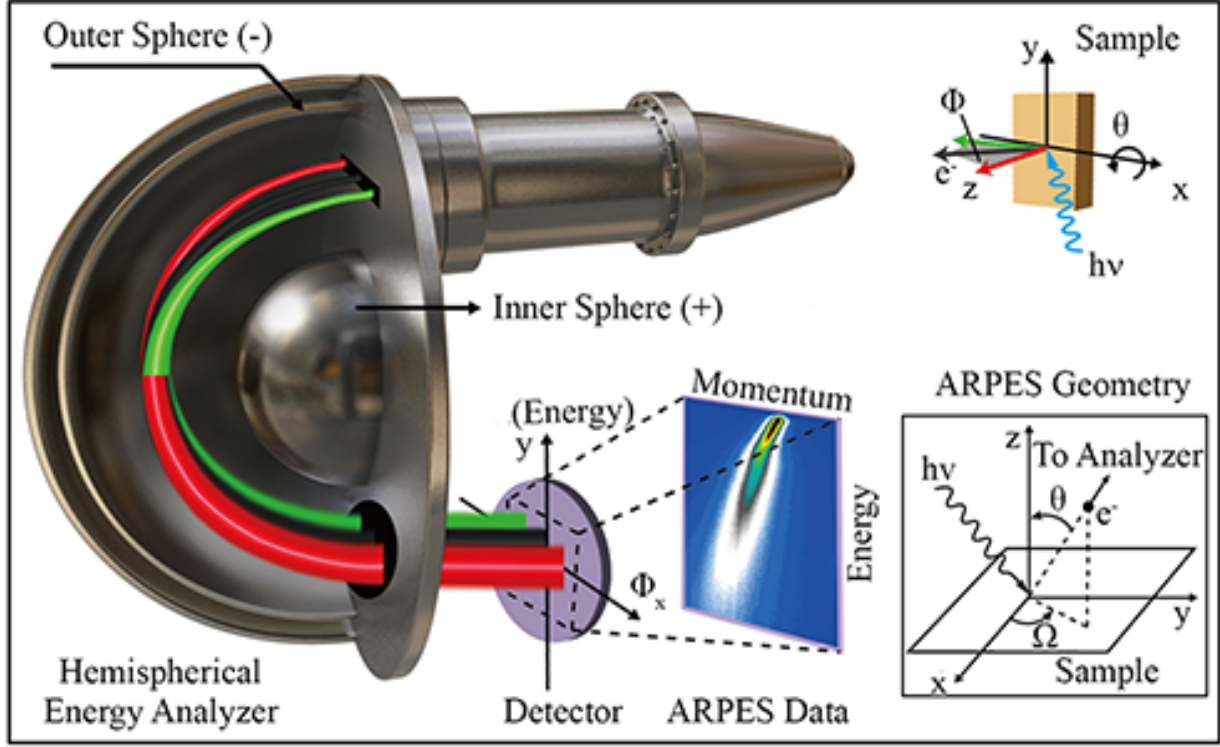


FIG. 1: Working principle of the angle-resolved photoemission with hemispherical electron energy analyzer. The inset shows the measurement geometry of the angle-resolved photoemission process.

TABLE I: Some typical laser light sources used in ARPES

Laser Category	Generation	Application	Pho. Energy (eV)	Pulse width (ps,fs)	Rep. Rate (kHz,MHz)	Max.Pho.flux (photons/s)	Energy Res. (meV)	Tem. Res. (fs)	Refs	Remarks
Quasi-CW	NLO crystal SFG+SHG	High-Res ARPES	7	~10ps	80MHz	1.5×10^{15}	0.26meV	/	G.D.Liu et al.[21]	a
			6	~70fs(seed)	100MHz	$\sim 10^{15}$	4.7meV	/	J.D.Koralek et al.[20]	b
			7	~10 ps	120MHz	unknown	0.025meV	/	K.Okazaki et al.[186]	c
			5.3-7	5 ps	76MHz	$\sim 10^{14}$	unsecified	/	R.Jiang et al.[87]	d
CW	NLO crystal SFG+SHG	High-Res ARPES	6.05	infinite	infinite	1×10^{15}	0.01	/	A.Tamai et al.[37]	e
			6.49	infinite	infinite	1.25×10^{15}	$\sim 10^{-7}$ meV	/	M. Scholz et al.[54]	f
Pulsed Laser	NLO crystal SFG+SHG	Tr-ARPES	1.5,6	50 fs,160 fs	80MHz	unspecified	<22meV	163 fs	J.A.Sobota et al.[41]	g
			1.5,6.04	35 fs,55 fs	250kHz	$\sim 10^{13}$	40meV	65 fs	J.Faure et al.[40]	
			1.48,5.92	170 fs,-	250kHz	unspecified	≥ 10.5 meV	≥ 240 fs	Y.Ishida et al.[149]	
HHG	Noble gas HHG	Tr-ARPES	1.58,15-40	40 fs,100 fs	10kHz	3.6×10^{17}	90meV@35.6eV	125 fs	B.Frietsch et al.[43]	h
			1.6,22.1	30fs,11 fs	10kHz	unspecified	170meV	13 fs	G.Rohde et al.[42]	i
			1.57,20.4	30 fs	1kHz	unspecified	unspecified	30 fs	J.C.Petersen et al.[31]	
Mod./Reson. type HHG	Mixed rare gas	High-Res ARPES	10.5	10 ps,	0.2-8MHz	9×10^{12}	< 1meV	/	M.H.Berntsen et al.[75]	j
			10.9	100 ps,	1-20MHz	$\times 10^{13}$	< 2meV	/	Yu He et al.[76]	k
FEL	Long Undulator	Tr-ARPES	26-300	30-150 ps	<10Hz	Very high	300 meV	700 fs	S Hellmann et al.[59]	

(a). First high resolution VUV-laser ARPES. (b). First high resolution UV-laser ARPES. (c). The highest resolution VUV-laser ARPES. (d). Tunable laser ARPES. (e). First CW UV laser ARPES. (f). First CW deep-UV laser for ARPES. (g). Quasi-CW laser tr-ARPES. (h). Good energy and time resolution compromised tr-ARPES. (i). Very high time-resolution tr-ARPES. (j). First high resolution HHG-laser ARPES. (k). First high resolution resonant type HHG-laser ARPES.

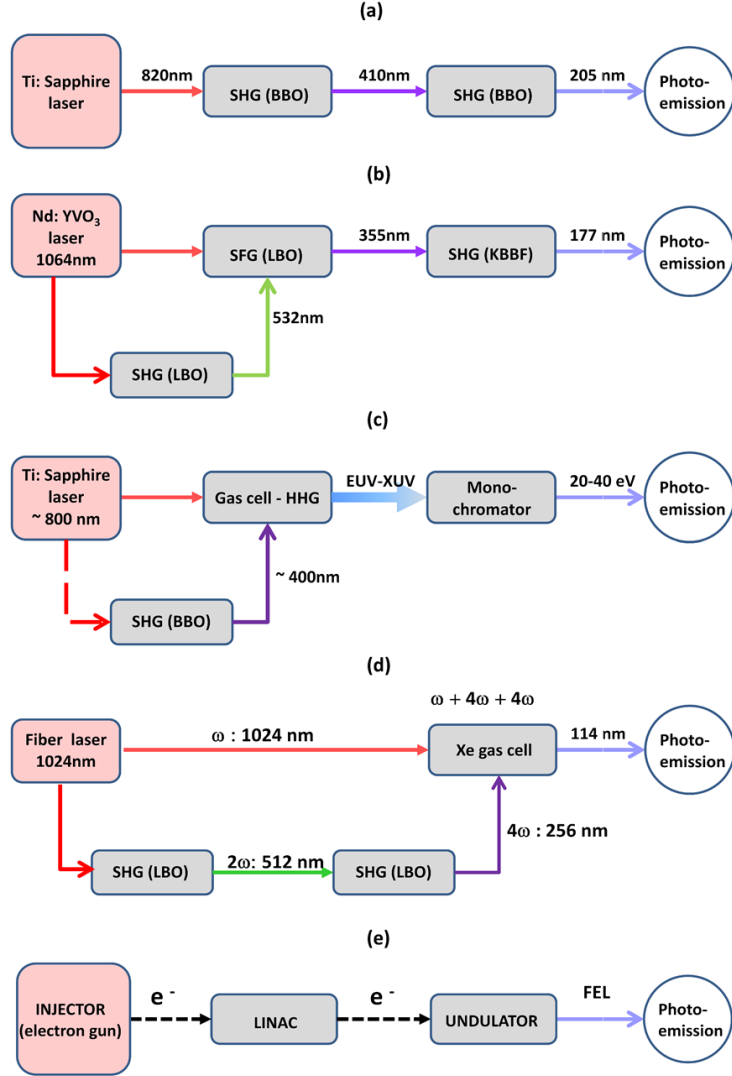


FIG. 2: Schematic layout of the working principles for different laser sources. (a). For pulsed 100 kHz UV laser (fs-version and ps-version) and CW UV laser. (b). For Quasi-CW VUV laser ~ 100 MHz and pulsed ~ 100 kHz. (c). For HHG laser: $1 \sim 100$ kHz. (d). For the Resonance-type HHG: ~ 200 kHz - 50 MHz. (e). For free electron laser.

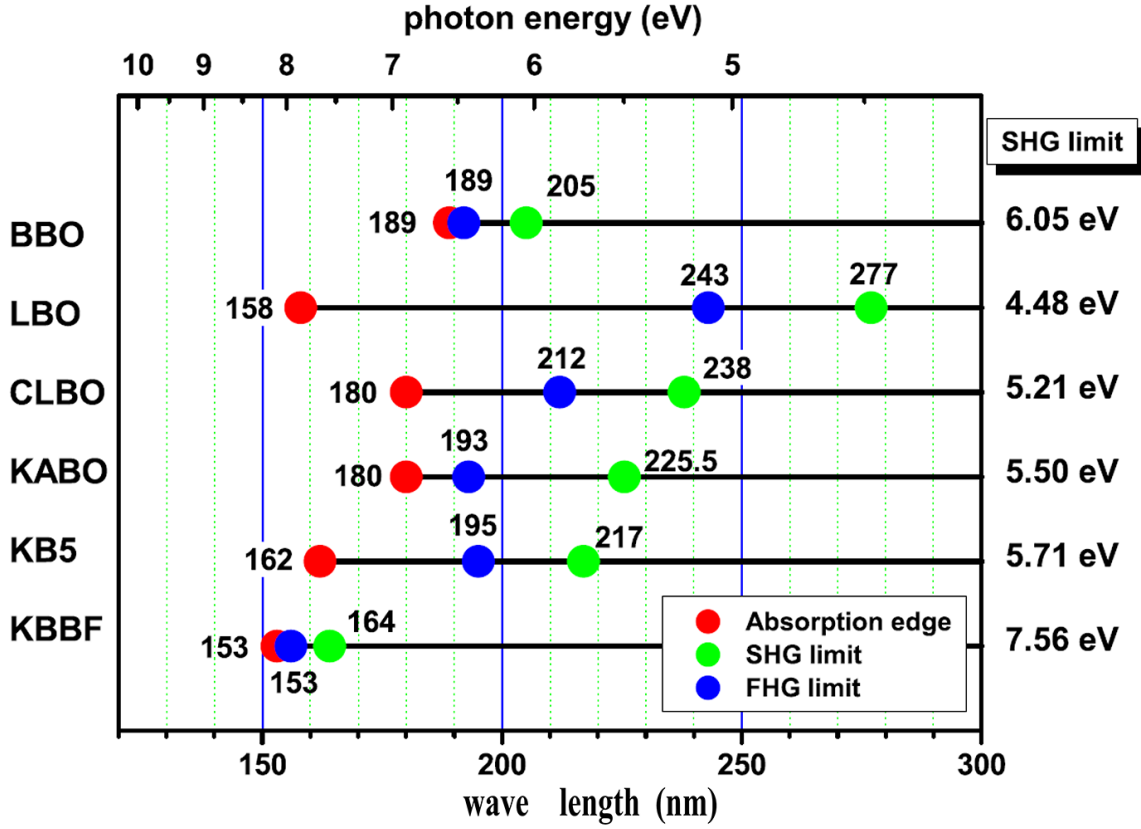


FIG. 3: A summary of some typical NLO crystals and their SHG limit, FHG (fourth harmonic generation) limit, and absorption edge[21]. The shortest SHG wavelength (highest SHG energy) is only available for KBBF crystal among all the NLO crystals.

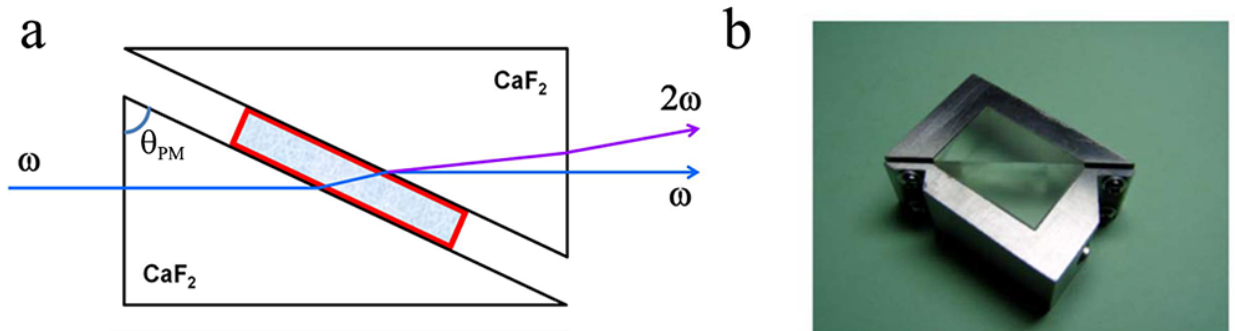


FIG. 4: (a). The schematic sandwich structure of an optically contacted, prism-coupled KBBF crystal device. (b). A photo of a typical KBBF- CaF_2 prism-coupled device.

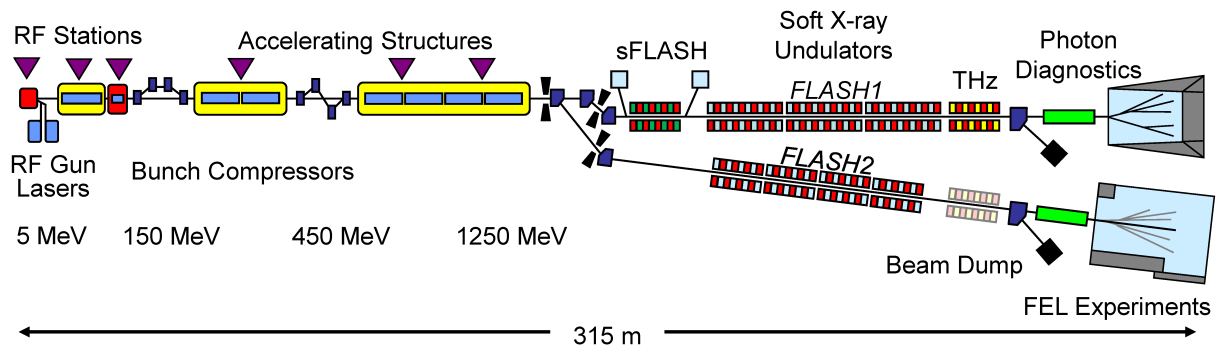


FIG. 5: A schematic layout of the first XUV and soft X-ray FEL apparatus FLASH[61].

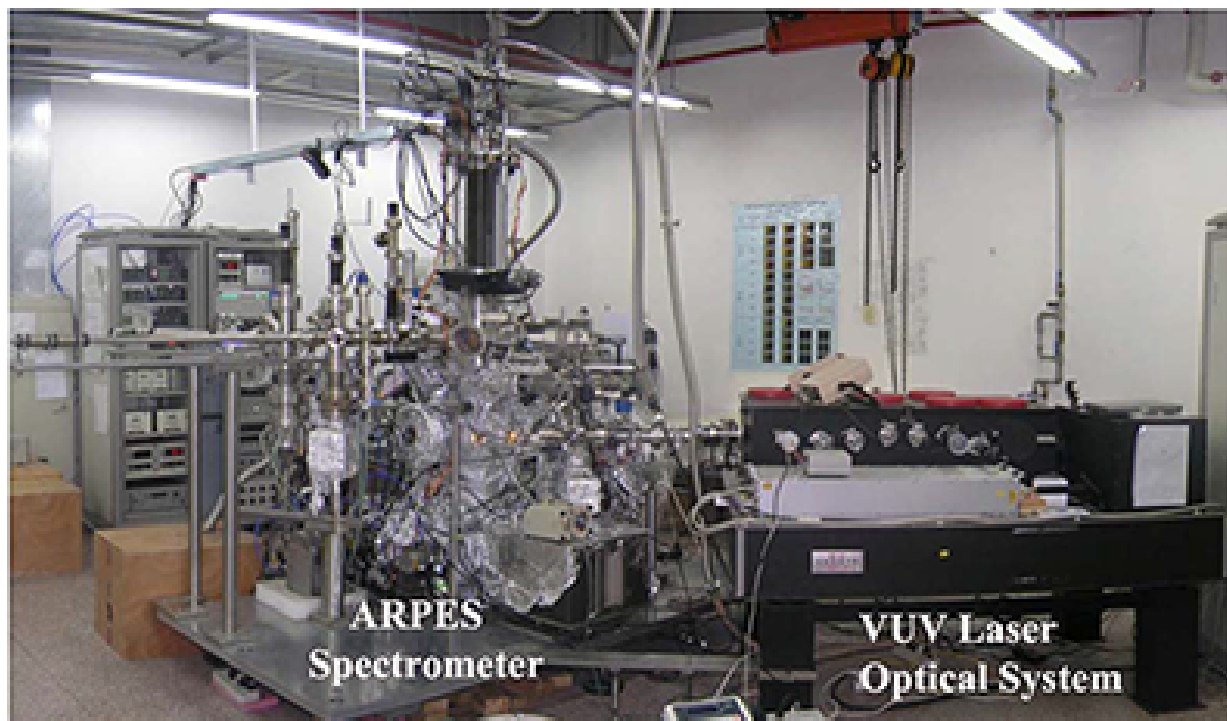


FIG. 6: A photograph of the VUV laser-based ARPES system.

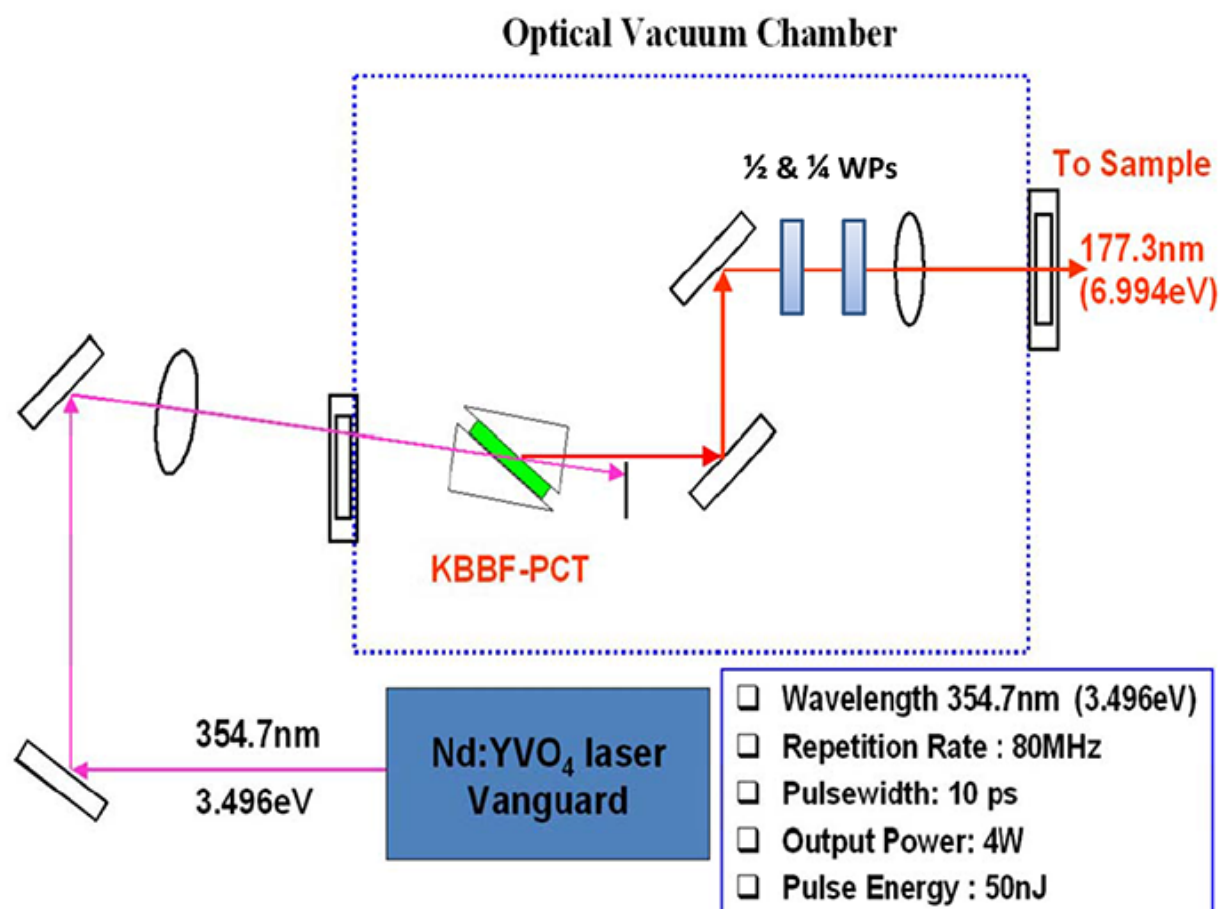


FIG. 7: A schematic layout of a VUV laser optical system[21].

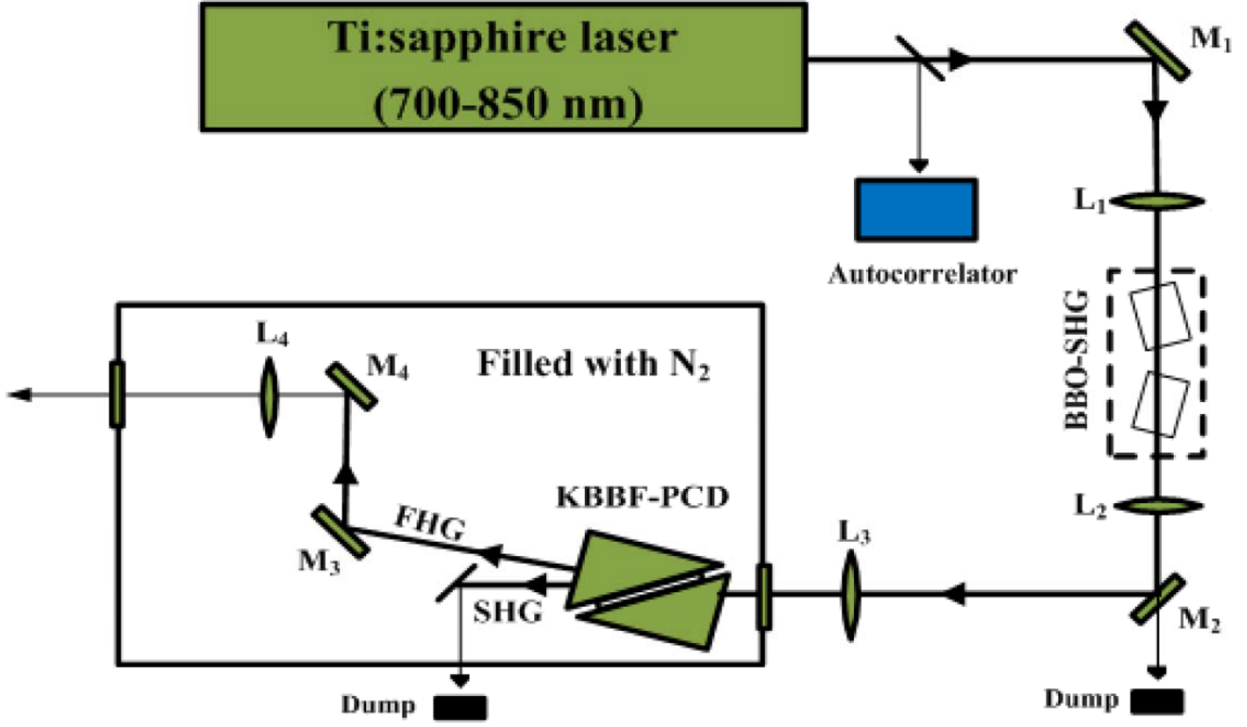


FIG. 8: A schematic layout of a tunable and deep-UV laser optical system[85].

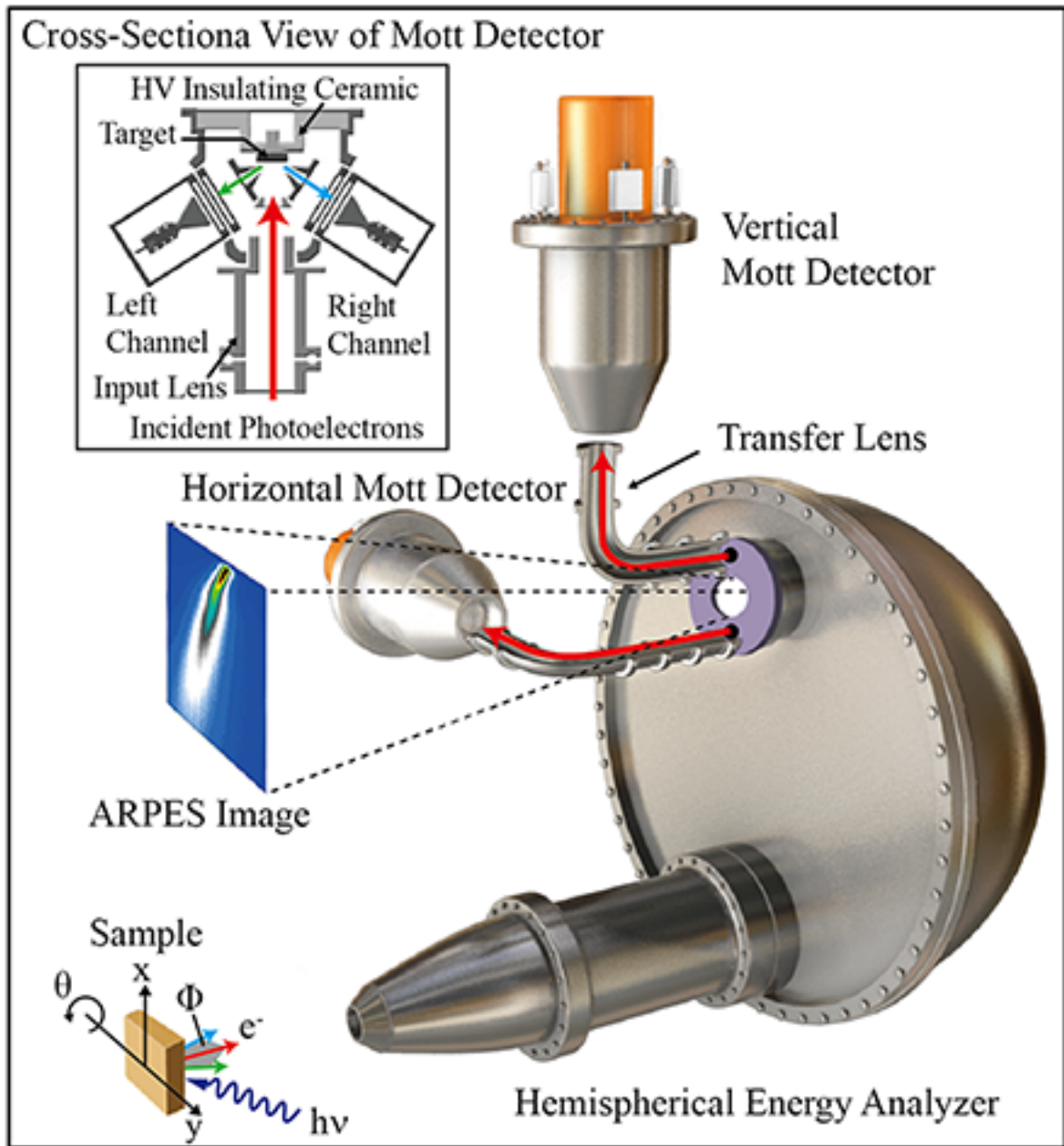


FIG. 9: Working principle of a spin-resolved ARPES equipped with two Mott type spin detectors. The inset is the cross-sectional view of the Mott detector.

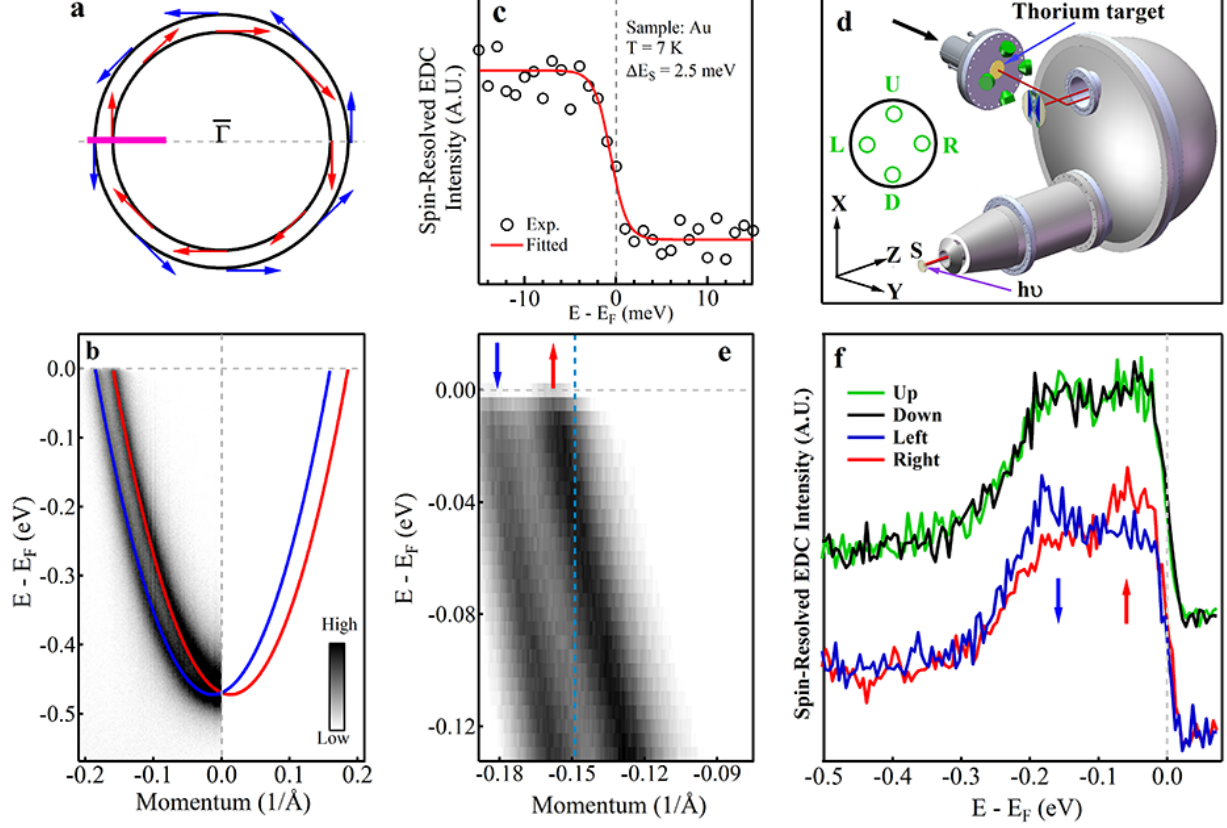


FIG. 10: The spin-resolved ARPES measurements on the Au(111) surface state[47]. a. Schematic Fermi surface and associated spin texture of the Au(111) surface state. b. Schematic band structure of the Au(111) surface state along the momentum cut shown in a as a dashed line. It is overlaid on the band structure measured by regular ARPES (left half of the momentum range). c. Spin-resolved energy resolution test obtained by measuring the Fermi edge of a clean polycrystalline Au at 7 K. The measured data (open circles) are fitted by the Fermi distribution function (red solid line) and the overall fitted line width is 3.52 meV. By removing the thermal broadening, an instrumental spin-resolved energy resolution of 2.5 meV is obtained. d. Schematic layout for a SARPES system which combines a Scienta R4000 electron energy analyzer with a Mott-type spin detector. e and f show, respectively, the band structure image and the four spin-resolved EDCs of the Au(111) surface state obtained simultaneously by the SARPES system. The corresponding momentum cut for the image (e) is shown in (a) as a pink thick line. The corresponding momentum point for the spin-resolved EDCs (f) is shown in (e) as a dashed blue line.

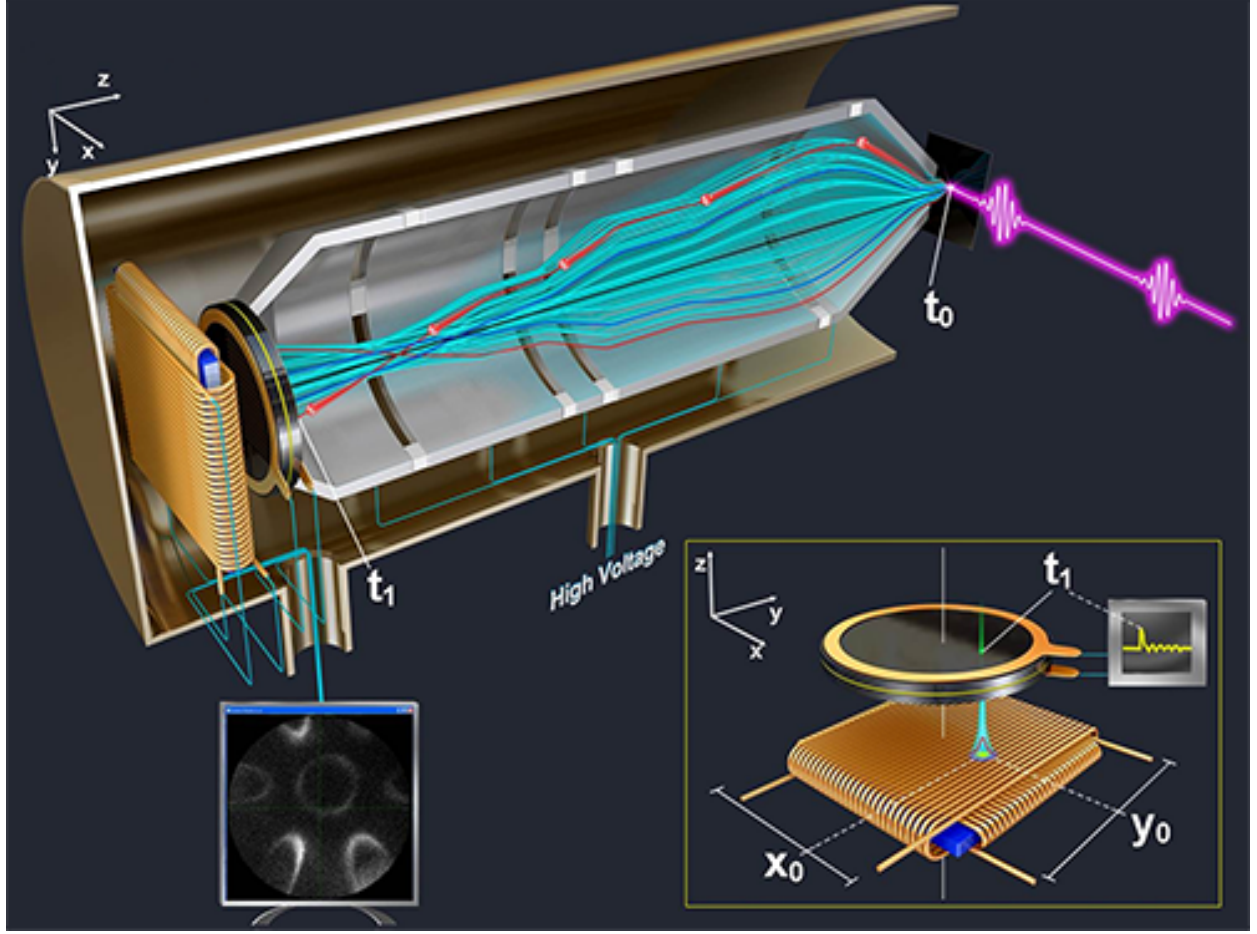


FIG. 11: Schematic 3D drawing of a 7 eV VUV laser-based ARToF-ARPES system. The analyzer consists of an electrostatic lens system and a MCP/DLD detector attached at the end of the lens. The light-blue lines represent the photoelectron trajectories inside the lens. The MCP/DLD will read out information of the arriving time and arriving location on the detector for each photoelectron, thus can be used to determine the electron energy and emission angle. The bottom-right corner inset shows a zoom-in view of the MCP/DLD unit.

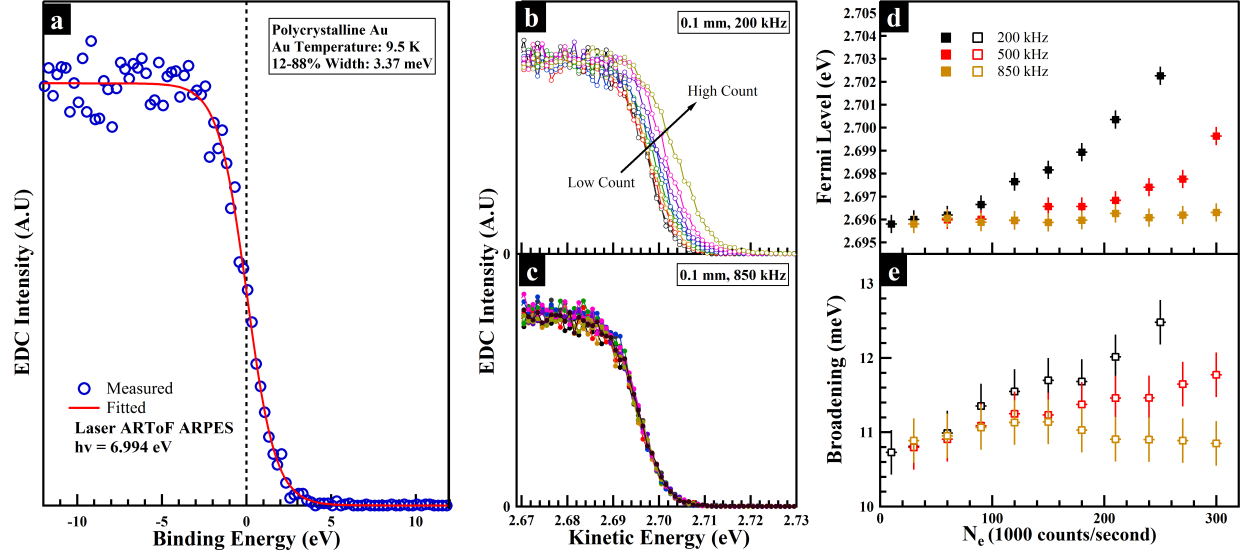


FIG. 12: Testing results of the VUV-laser-based ARToF-ARPES system. (a). EDC from measuring on a polycrystalline Au by using 6.994 eV laser light at 9.5 K. The measured Fermi edge width is ~ 3.37 meV. After removing the contribution from temperature, the overall instrumental energy resolution obtained is better than 1 meV. (b) and (c) are the polycrystalline Au EDCs taken at two different laser repetition rates. The fitted results of the Fermi level position and corresponding Fermi edge width are summarized in (d) and (e). It is clear that as one increases the operating repetition rate of the laser light, the space charge effect can be strongly suppressed.

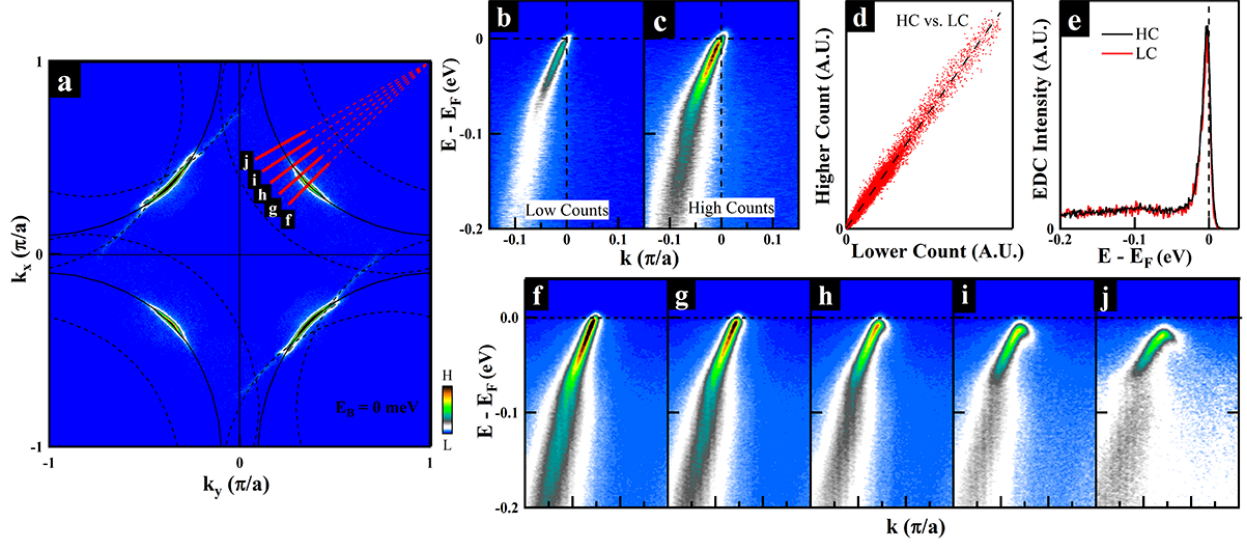


FIG. 13: Fermi surface and band structure of Bi2212 measured by VUV laser-based ARToF-ARPES. (a). Fermi surface measured by ARToF-ARPES with 6.994 eV laser light. The solid and dashed thin lines are simulated Fermi surface and related superstructure replicas, respectively, within the first Brillouin zone. (b, c) are two band structures measured along the nodal direction with low count rate and high count, respectively. (d) is the scatter plot (red scatters) showing the linear scaling relationship between the count rate at each pixel from both measurements. (e). EDCs from (a-c) at the same Fermi momentum measured using low and high count rates. They match each other very well after scaling their intensity. Both (d) and (e) indicate little nonlinearity for the ARToF analyzer. (f-g). Band structure taken along the momentum cuts shown in (a) that all extend to the (π, π) point.

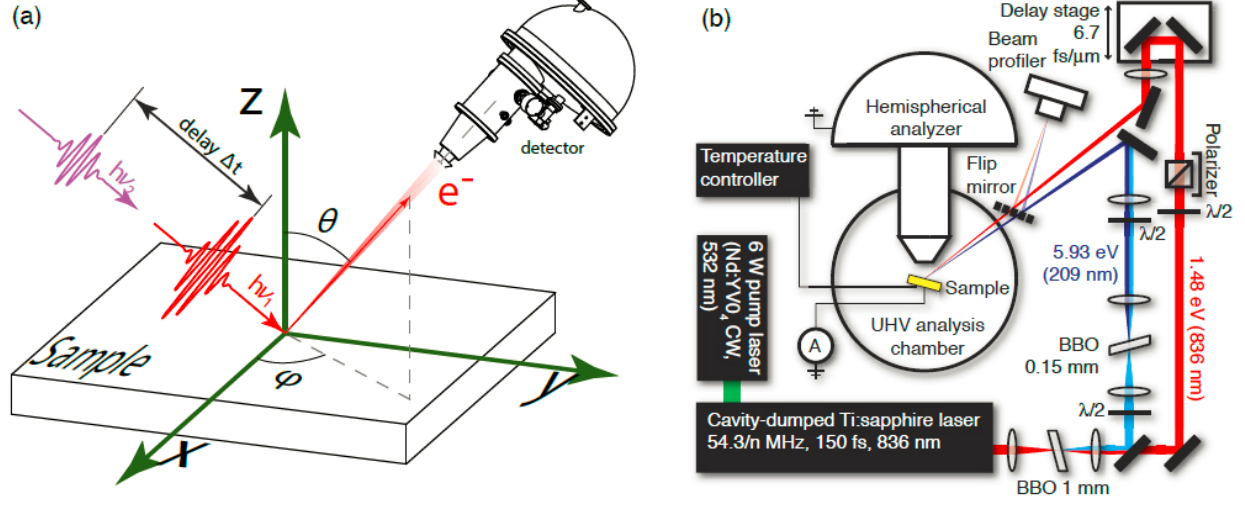


FIG. 14: (a) Schematic of a time-resolved ARPES. (b) A typical setup of time-resolved ARPES based on solid laser source[133].

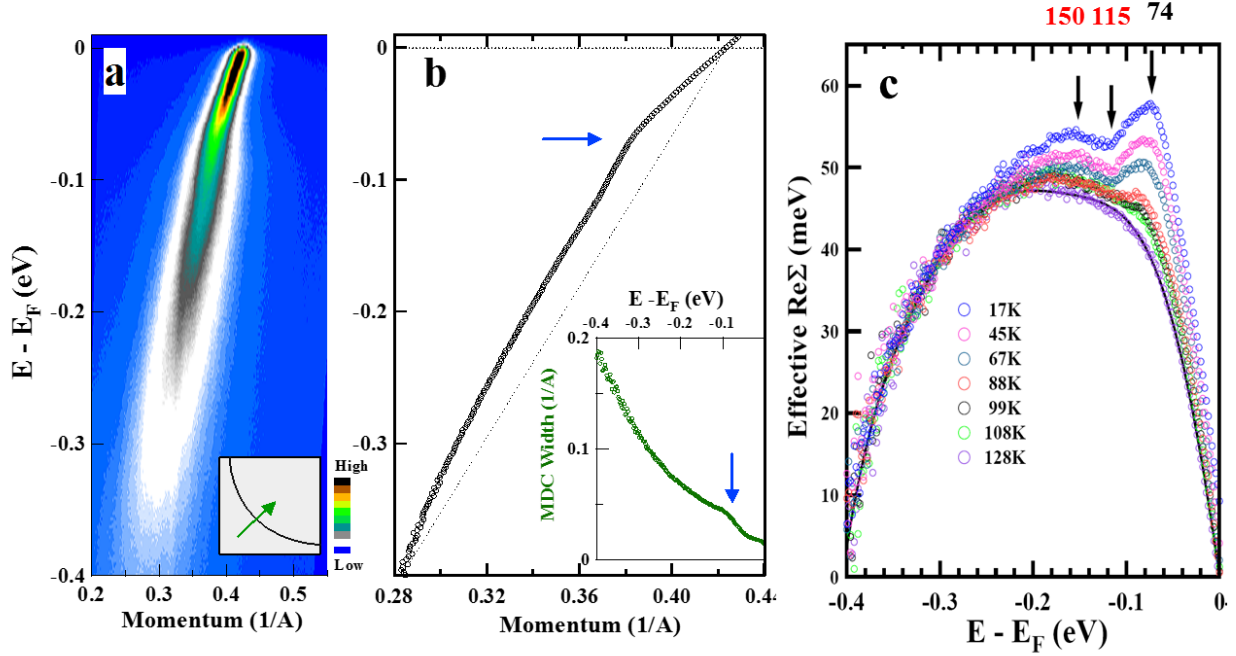


FIG. 15: Electronic structure of Bi2212 from VUV-laser ARPES[163]. (a). Band structure of Bi2212 taken along the nodal direction. (b). Quantitative dispersion and scattering rate obtained by MDC fitting of the original data (a). (c). The effective real part of electron self-energy at different temperatures. It is clear that there are two high energy features at 115 meV and 150 meV in addition to the well-known 70 meV mode-like feature.

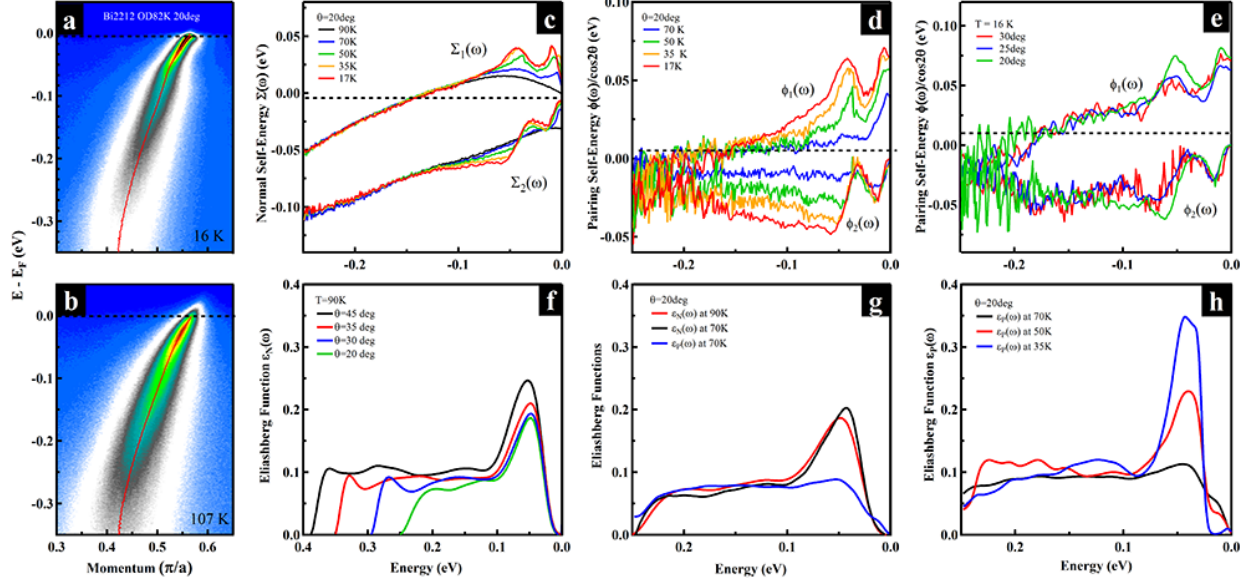


FIG. 16: Extraction of Eliashberg functions from VUV laser-based ARPES on Bi2212[171]. (a) and (b) are high resolution ARPES data from over-doped Bi2212 with a $T_c=82$ K measured at 16 K and 107 K, respectively. (c). Normal electron self-energy; (d) is pairing self-energy at different temperatures for a given cut. (e) is pairing self-energy at different momentum cuts for a given temperature. (f). The extracted normal Eliashberg function for different momentum cuts. (g). Extracted normal Eliashberg function and pairing Eliashberg function for Bi2212. (h). Extracted pairing Eliashberg function for Bi2212.

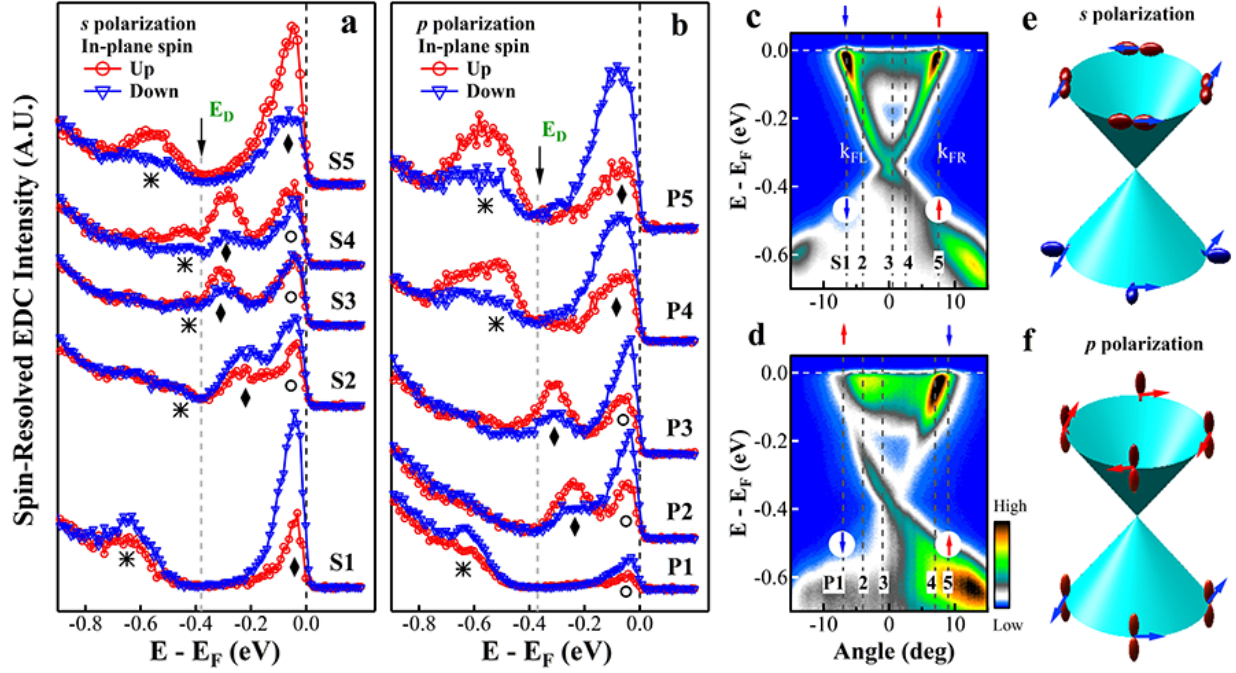


FIG. 17: SARPES measurements of Bi₂Se₃ topological insulator under different polarization geometries[47]. a. Spin-resolved EDCs at five representative momenta along the $\bar{\Gamma}\bar{K}$ momentum cut under the *s* polarization geometry. The corresponding momentum points are marked as the dashed lines in the band image measured from regular ARPES under the *s* polarization geometry (c). The EDC peaks corresponding to the bulk band, the upper Dirac cone and the lower Dirac cone are marked by empty circle, solid diamond and asterisk, respectively. (b). Spin-resolved EDCs at five representative momenta along the $\bar{\Gamma}\bar{K}$ momentum cut under the *p* polarization geometry. The corresponding momentum points are marked as the dashed lines in the band image measured from regular ARPES under the *p* polarization geometry. (d). On the right side of **c**, the measured spin and orbital texture under the *s* polarization geometry is sketched for both the upper Dirac cone and the lower Dirac cone. On the right side of **d**, the spin and orbital textures under the *p* polarization geometry is sketched.

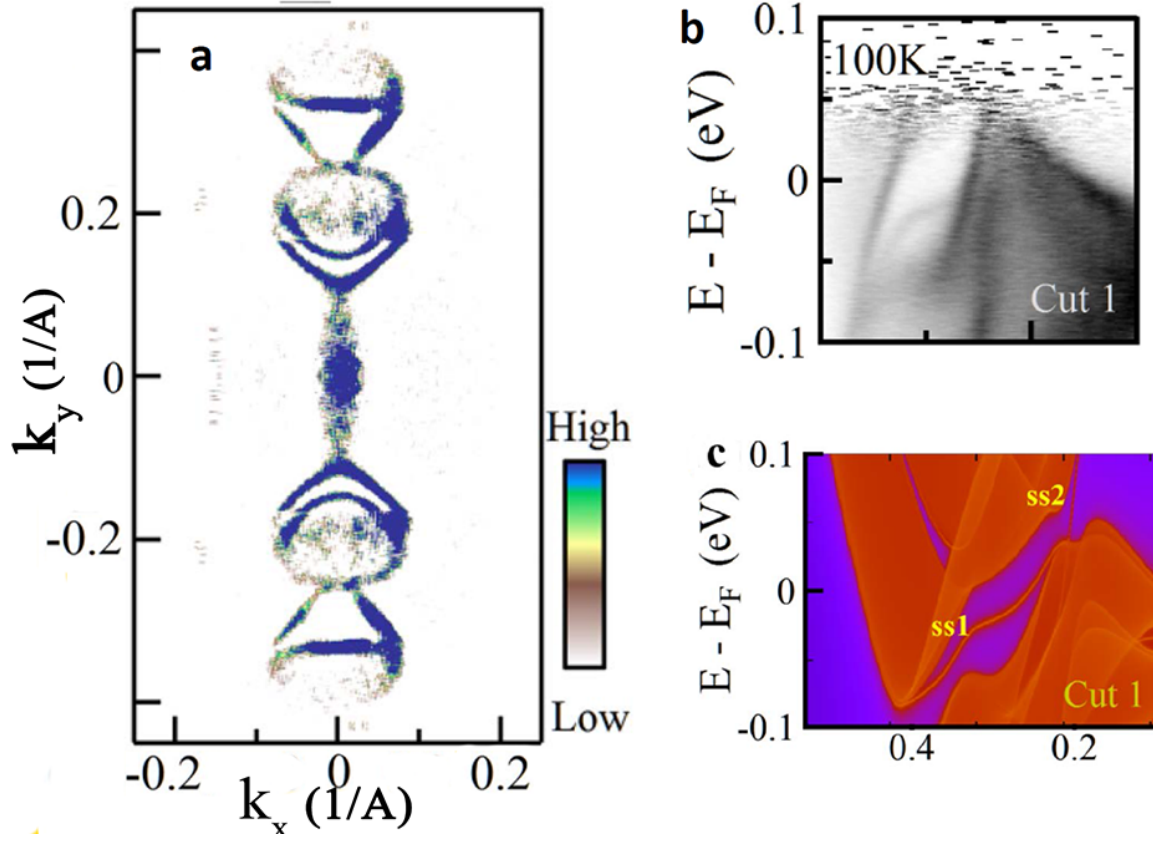


FIG. 18: Complete electronic structure of WTe₂ from VUV laser-based ARToF-ARPES measurements[48]. (a). The measured complete Fermi surface of WTe₂. (b). Observation of the surface state band at 100 K. (c). Calculated band structure.

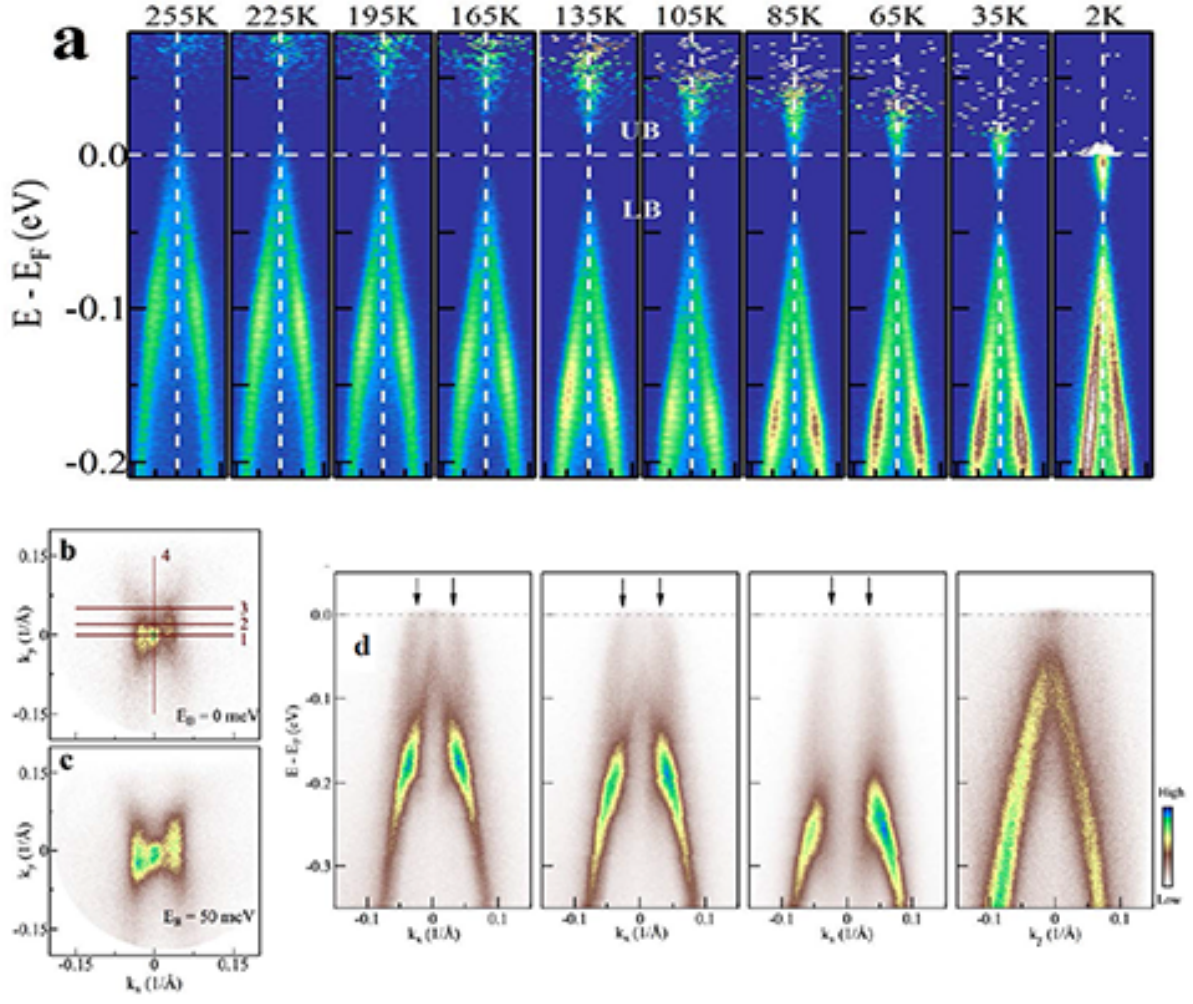


FIG. 19: Temperature-induced Lifshitz transition and topological nature of ZrTe₅ from VUV laser-based ARTof-ARPES measurements[86]. (a). Temperature evolution of the band structure in ZrTe₅; (b). Observation of weak topological insulator feature, the one-dimensional-like streaks, in some ZrTe₅ samples.

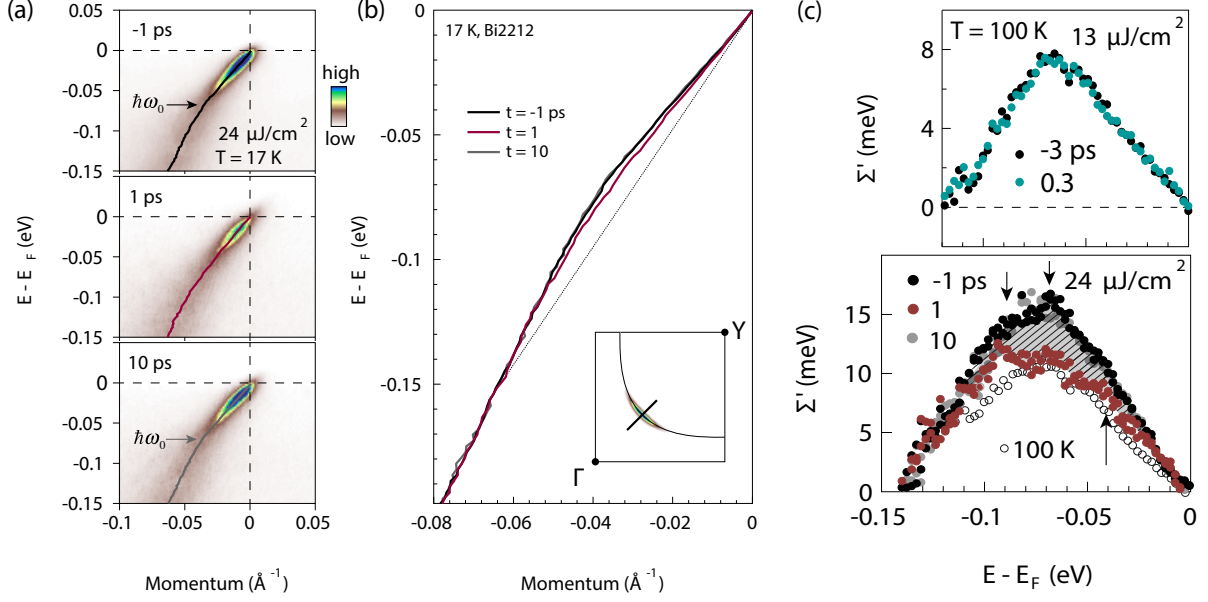


FIG. 20: Time-resolved ARPES data of an optimally-doped Bi2212 sample ($T_c = 91$ K) measured along a nodal cut ($\Gamma(0, 0) - Y(\pi, \pi)$ direction)[137]. (a). Equilibrium (before pumping, $t = -1$ ps), transient (after pumping, $t = 1$ ps and $t = 10$ ps) photoelectron intensity (represented by false color) as a function of energy and momentum, for a pump fluence of $24 \mu\text{J}/\text{cm}^2$. The bold solid black lines are the momentum distribution curve dispersions at the corresponding delay time. The arrows mark the position of the kink at ~ 70 meV. (b). MDC dispersions for different delay times (-1 , 1 , and 10 ps). (c). The effective real parts of the electron self-energy at 100 K (upper panel) and at 16 K (lower panel).

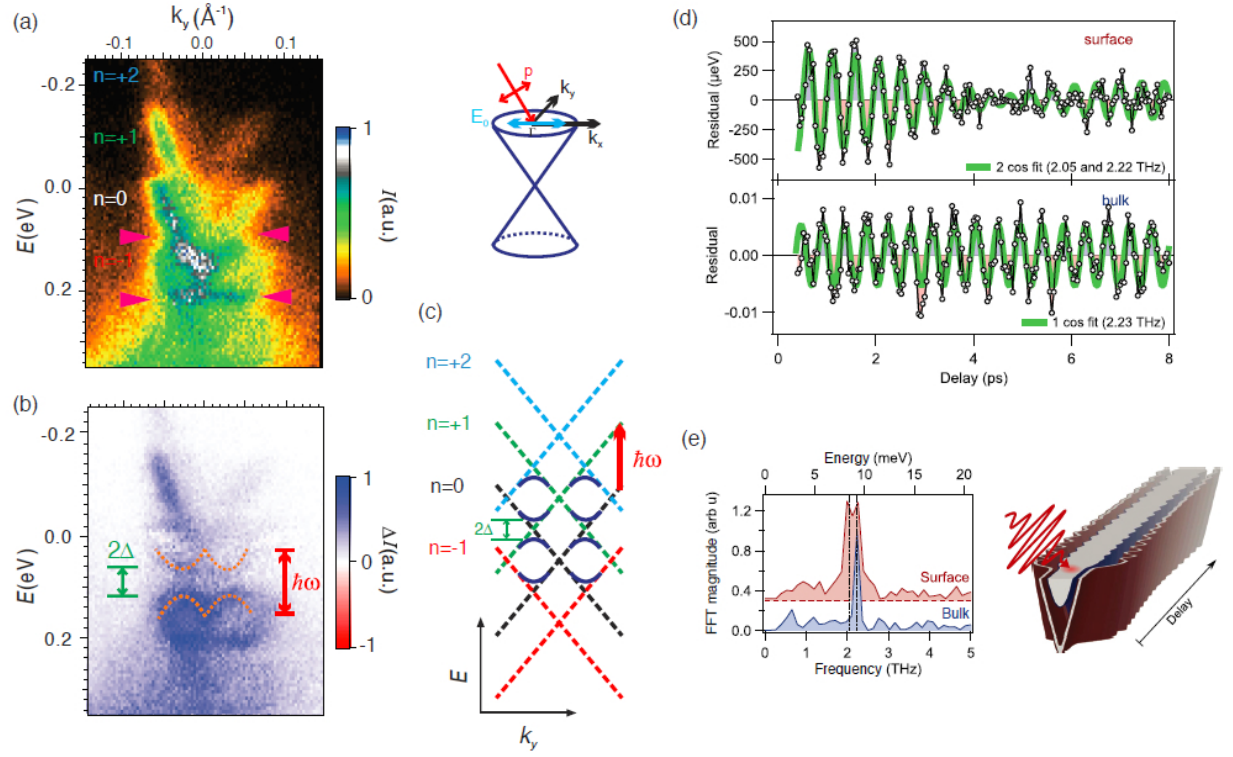


FIG. 21: Time-resolved ARPES data of a Bi_2Se_3 sample. (a). The time-resolved ARPES data through Γ along the k_y direction pumped with linear polarized pulse[181]. (b). The same data after subtracting the data at $t = -500$ fs[181]. (c). Sketch of the side bands of different order[181]. (d). Pump-induced electronic dynamics in surface bands (upper panel) and bulk bands (lower panel)[142]. (e). Fourier transforms of the spectra shown in (d) (left) and cartoon depiction of the optical excitation of coherent phonons in the bulk and surface bands (right)[142].